A STUDY OF THE MESOSCALE PRECIPITATION PATTERNS ASSOCIATED WITH THE NEW ENGLAND COASTAL FRONT

by

FRANK DECATUR MARKS, Jr.

SUBMITTED IN PARTIAL FULFILLMENT OF THE
REQUIREMENTS FOR THE DEGREE OF MASTER OF SCIENCE
at the
MASSACHUSETTS INSTITUTE OF TECHNOLOGY
July, 1975

Signature of Author .....
Department of Meteorology, July 1975

Certified by .....
Thesis Supervisor

Accepted by .....
Chairman, Departmental Committee on Graduate Students
Lindgren

A STUDY OF THE MESOSCALE PRECIPITATION PATTERNS ASSOCIATED WITH THE NEW ENGLAND COASTAL FRONT

by

Frank Decatur Marks, Jr.

Submitted to the Department of Meteorology on 2 July 1975 in partial fulfillment of the requirements for the degree of Master of Science.

ABSTRACT

Characteristics of the precipitation were studied for six storms where mesoscale coastal fronts developed in eastern New England. In all six cases, the principal larger mesoscale precipitation features were bands associated with the large scale baroclinically-induced circulation. Typically, the precipitation in these bands developed in convective clouds which were embedded in a layer of cold dry mid-tropospheric air and had their "roots" in a layer of warm saturated air just below.

The coastal front, in all six cases, developed locally in the planetary boundary layer and tended to lie along a line between Boston, Massachusetts and Providence, Rhode Island. The coastal fronts had a depth of approximately 300 meters and durations of 7 to 15 hours. Their development was independent of the large scale baroclinically-induced circulation. In every case precipitation falling in the observed bands was enhanced in the coastal front region. Typical values of the enhancement were 20-30 percent, with a range from near 0 percent to 196 percent.

The mechanism which caused the enhancement is hypothesized to be low-level growth of hydrometeors through accretion in clouds produced by convergence of water vapor and lifting associated with the coastal front circulation in the boundary layer. Results of computations of the observed surface water vapor convergence and of cloud depths and liquid water contents necessary to produce the observed enhancement indicate that this hypothesis is a very reasonable one.

In one case another mesoscale feature, a low-level jet, was the principal mechanism affecting the precipitation distribution.

Thesis Supervisor: Dr. Pauline M. Austin
Senior Research Associate

TABLE OF CONTENTS

LIST OF TABLES

LIST OF FIGURES

FIGURE 6: The hourly precipitation distribution for representative stations in the four regions investigated (see Table 2), 8 December 1969. The abscissa is time (Z) and the ordinate is precipitation (mm). The times that the CsF and the three labeled bands (a,b,c) were present are indicated by brackets.

FIGURE 7: Tracks of the two SMSA's associated with the low-level jet, 15 February 1970, is shown at intensity level five (2mm hr^{-1} in snow). The circle has a radius of 200 km and the lines show the direction of motion. (a) The first SMSA shown at 21Z, 22Z, and 23Z; (b) the second SMSA shown at 22Z and 23Z.

FIGURE 8: PPI tracing of the SMSA's, associated with the low-level jet, at 2245Z, 15 February 1970. The outer circle is 200 km in radius, the middle circle at 100 km radius, and the innermost one at approximately 10 km showing the ground clutter extent. The light solid line indicates the threshold of intensity level 3 (~0.5mm hr^{-1} in snow), the heavy solid line level 4 (~1mm hr^{-1} in snow), the cross-hatched area level 5 (~2mm hr^{-1} in snow), and the solid area level 6 (~3mm hr^{-1} in snow).

FIGURE 9: The same as Figure 6, except for the case of 15 February 1970. The times of the CsF and the jet

are indicated by brackets. The two SMSA's associated with the jet are labeled (d) and (e).

FIGURE 10: PPI tracing of SMSA over Boston at 0030Z, 24 December 1970. The circles are the same as in Figure 8. Stippling represents the threshold of the lowest intensity level.

FIGURE 11: RHI- derived cross-section through SMSA for 0100Z, 24 December 1970. The abscissa is distance from the radar (km) and the ordinate is height (km). The light solid line is the threshold of intensity level one; the heavy solid line intensity level two (0.2mm hr^{-1} in snow); cross-hatching level 3 (~0.5mm hr^{-1} in snow); and solid level 4 (~5mm hr^{-1} in snow).

FIGURE 12: The same as Figure 6 except for case of 24 December 1970. The times of the CsF and the SMSA are indicated by brackets. Letters indicate bands that were observed.

FIGURE 13: Mean water vapor divergence field over 15 hours when CsF was present for case of 24 December 1970. Solid lines represent isopleths of water vapor divergence at intervals of 6×10^{-5} g m^{-3} sec^{-1}. Positive values indicate divergence and negative values convergence.

FIGURE 14: Same as Figure 4, except for 00Z, 24 December 1970.

FIGURE 15: Schematic representation of cross-section through surface layer during times the CsF is present. The abscissa is distance (km) and the ordinate is height (km). The stippled areas represent the frontal zones and the broken lines represent the water vapor convergence field.

FIGURE 16: Combinations of cloud depth and mean liquid water contents, which would add 0.90mm hr^{-1} of water to an initial snowfall of 0.46mm hr^{-1}.

I. INTRODUCTION

A. The Problem

The apparent lack of an increase in the skill of daily forecasts, despite the continuous improvement of the predicted synoptic-scale flow patterns at the surface and 500 mb, discussed by Sanders (1973), suggests that more effort should be applied toward investigations of various mesoscale phenomena and their impact on routine local forecasts. One type of mesoscale phenomenon, the New England Coastal Front (from here on referred to as the CsF), has been discussed in papers by Bosart et. al. (1972) and Bosart (1975). The CsF is a very localized phenomenon that poses a number of problems to forecasters. It forms in the cold air ahead of a surface cyclone center, and the major problem it poses is usually in forecasts of precipitation amount and type. This problem arises as a result of the CsF's position, downstream of the cyclone center where the bulk of the storm's baroclinically-induced precipitation occurs.

In case studies of the CsF, Bosart and his colleagues noted a tendency for a maximum in the total storm precipitation just on the cold side of these fronts. They suggested that the intensification of the thermally direct circulation, associated with these fronts would enhance the precipitation in this region. They also noted, however, that the temporal and spatial density of the reporting stations was not really adequate to resolve the nature of the enhancement.

Other investigators (Austin and Houze, 1972; Kreitzberg and Brown, 1970; Reed, 1972; Browning et. al., 1973; and Harrold, 1973) have used quantitative radar data as a tool to derive the nature and movement of mesoscale precipitation patterns associated with various baroclinic disturbances. To obtain the characteristics of the precipitation patterns, the combination of quantitative radar data with hourly rain gauge amounts, standard synoptic-scale rawinsonde, and surface observations has proven to be quite a successful approach. A similar approach will be used in this study.

The aim of the study is to explore the extent and manner in which precipitation patterns are affected by a CsF circulation. An attempt will be made to identify the larger mesoscale precipitation features that contribute to the overall precipitation pattern. The extent to which these features, and subsequently the amount and distribution of precipitation, are influenced by the CsF circulation or the large-scale baroclinic disturbance respectively, will be determined.

B. The Coastal Front

The CsF, as described by Bosart et. al. (1972) and Bosart (1975), is a unique phenomenon which occurs in only a few locations around the world. These locations must combine a coastal geographic location backed by mountains inland and a certain coastal configuration discussed by Bosart. Southern New England has all the necessary features.

In New England, the CsF is predominantly a late fall, early winter phenomenon. It forms in the planetary boundary layer along the southeastern coast, with a tendency to lie along a line between Boston, Massachusetts and Providence, Rhode Island.

The surface synoptic field associated with its development is dominated by a cold anticyclone to the north and east of New England. This provides a mean easterly geostrophic flow at low levels which causes a shallow dome of cold air to be dammed up east of the mountains in Central New England. Along the coast, it is characterized by relatively strong horizontal temperature gradients (as high as 5-10 C over 5-10 km), between the cold air and the relatively warm air over the water).

The CsF serves as a boundary, characterized by a cyclonic wind shift, between a light northerly flow ($\leq$ 5 m sec^{-1}) of cold air over land and a stronger easterly flow ($\sim$ 10 m sec^{-1}) of maritime air over water. The differential friction between the flow over the land and that over the water has been proposed as the mechanism to produce the deformation and convergence fields favorable for frontogenesis.

C. Characteristics of Mesoscale Precipitation Features

To identify the mesoscale precipitation features in a CsF situation, it is necessary to know what the typical characteristics of these features are.

Austin and Houze (1972) used quantitative radar data to obtain a description of the nature of precipitation patterns in New England storms. Four distinct scales of precipitation areas were described: synoptic areas, size scale larger than 10^4 km^2, and a lifetime from one to several days; large mesoscale areas (LMSA's), size scale ranging from 10^3 - 10^4 km^2, and a lifetime of several hours; small mesoscale areas (SMSA's), size scale ranging from 100 - 400 km^2, and a lifetime of about an hour; and cells, size scale around 10 km^2, and lifetimes on the order of a few minutes. They found that these precipitation areas were highly organized with the larger scale areas always containing at least one area of the smaller scales. The motions and relative intensities of these areas also showed a consistent pattern.

Austin and Houze found evidence that the SMSA's were closely related to cellular activity, but they could offer no hypothesis concerning the development of the LMSA's.

A number of investigators have looked at the movement and organization of LMSA's for various cyclonic storms. They have found that SMSA's tend to be organized to band-shaped areas several hundered kilometers long and thirty to forty kilometers wide. They have used combinations of rain gauge, radar, rawinsonde, and aircraft data to describe the bands and the three-dimensional structure of the atmosphere during the time they are present.

Studies by Browning et. al. (1973), Harrold (1973), Kreitzberg and Brown (1970), and Reed (1972) indicated that the bands first appeared at least 300 km ahead of the surface cyclone center and typically were associated with regions of convective activity moving in a region of convectively unstable air. This convectively unstable region developed when a tongue of cool dry mid-tropospheric air overran a layer of warm moister air moving near the surface and up over the warm frontal zone. Harrold (1973) chose to refer to this layer of warm moister air as the "conveyor belt" supplying moisture to the baroclinic circulation.

These bands were found to be typically aligned with the shear in the convectively unstable layer and to move approximately with the mean speed of this layer.

II. DATA AND METHOD OF ANALYSIS

A. Data

For this study the features of the CsF and the associated synoptic pattern are derived from regular hourly surface reports and NMC (National Meteorological Center) three-hourly surface analyses. The NMC three-hourly surface analyses are available on microfilm from NOAA/EDS (NOAA/Environmental Data Service).

The temperature and wind data, from the hourly surface reports for New England, were plotted and analyzed to determine the position and strength of the CsF. The hourly surface reports are received on a teletype circuit at the Department of Meteorology,

M.I.T. and are archived for a three year period.

The horizontal and vertical structure of the precipitation features are obtained using the WR-66 weather radar, operated by the Department of Meteorology at M.I.T. The radar's scopes display an averaged and range normalized signal which is quantized into intensity levels at intervals of 4.5 db. Each intensity level corresponds to an increase in precipitation rate of approximately a factor of two over the preceding level. The entire sequence of intensity levels on the PPI is photographed automatically every two to four minutes, depending on the number of intensity levels that are needed to describe the precipitation that is occuring. Approximately once an hour this process is interrupted in order to photograph a sequence of intensity levels from the RHI (Range-Height Indicator). The characteristics of the WR-66 radar are given in Appendix I.

The hourly precipitation amounts for New England stations were used to supplement the radar data in identifying the mesoscale precipitation structures and were the primary data in describing the total storm precipitation distribution for each case. There are approximately 70 reporting stations within the range of the radar. These data are published monthly by NOAA/EDS.

The vertical structure of temperature, humidity, and wind was obtained from the twelve-hourly rawinsonde ascents from the following stations: Portland, Maine (PWM); Albany, New York (ALB),

New York City Airport, New York (JFK); and Nantucket, Massachusetts (ACK), which was replaced by Chatham, Massachusetts (CHH) in mid-1970.

B. Selection of cases

Cases for the study were selected from a list presented by Bosart (1975) which contains fifty-seven cases for the eight year period 1964-1972. He classified them by synoptic situation into five types, A-E. Types A and B are characterized by developing cyclonic disturbances moving up the east coast of the United States. These types were associated with large amounts of precipitation. The other three types were rare, making up only a quarter of the smaple listed by Bosart. They were characterized by weak cyclones moving through New England and typically smaller precipitation amounts. Bosart's list appears in Appendix II.

The main constraint in the selection of cases for this study was the availability of quantitative radar data during the times the CsF was present. Because the quality of the radar data was significantly improved starting in the fall of 1969, only the cases after this time were considered. Storms that had good quantitative radar data during the times the CsF was present were chosen and are listed in Table 1.

The selected storms are exclusively type B cases. The reasons for this are probably two-fold. First, the type B situations make up almost fifty per cent of Bosart's list. Second,

these storms favor a lot of precipitation growth which would be detected more easily by the radar.

Also listed in Table 1 are two cases without a CsF taken from a study of precipitation patterns in extratropical cyclones by Reed (1972). Two of his storms were CsF cases and are included in this study. Two others without a CsF were added for comparison.

C. Methods of Analysis

1. Surface cyclone

The position and movement of the surface cyclone during the lifetime of the CsF was obtained from the NMC three-hourly surface analyses. In this study, the surface cyclone, associated with each case, was used to represent the synoptic-scale baroclinity of the atmosphere during the CsF lifetime.

2. Coastal front

Durations and positons of each CsF during its lifetime were determined through analysis of the hourly surface data for New England. The strength of the CsF was calculated by comparison of wind and temperature between various pairs of stations straddling the CsF. The pairs used were: Boston (BOS) and Worcester (ORH), Massachusetts (75 km apart); Boston (BOS) and Bedford (BED), Massachusetts (25 km apart); Portsmouth (PSM) and Concord (CON), New Hampshire (60 km apart); and Providence (PVD), Rhode Island and New Bedford (EWB), Massachusetts (45 km apart).

3. Mesoscale precipitation factors

The 35-mm films of the PPI displays were placed in a Richardson viewer, allowing the motion and spatial distribution of the storm's precipiation patterns to be observed. At approximately fifteen minute intervals, tracings were made of the entire PPI at all intensity levels. These were used together with direct viewing of the films to track identifiable features (LMSA's and SMSA's).

Tracks were determined from composites which show the positions of the identifed feature each half hour. Usually the features were best defined at intensity level four, which corresponds to a precipitation rate of approximately 0.5 mm hr^{-1} in snow and 5 mm hr^{-1} in rain.*

From these composites, the translational speed, direction of motion, and spatial distribution of the observed mesoscale precipitaion features were determined. The direction and speed of the mesoscale features (i.e. bands) for the two non-CsF cases were taken from Reed (1972).

---

* These precipitation rates were computed using the Gunn and Marshall (1958) Z-R relationship for aggregated snow flakes and the Marshall and Palmer (1949) Z-R relationship for rain drops. These are: for snow $Z = 2000R^{2.0}$; and for rain $Z = 200R^{1.6}$, where Z is the equivalent reflectivity factor ($mm^6 m^{-3}$) and R is the rainfall rate (mm hr^{-1}).

4. Vertical structure of the atmosphere

Vertical profiles of wind and thermodynamic variables were obtained from rawinsonde ascents for the stations nearest in time and space to the observed mesoscale precipiation features. The wind was separated into u- and v-components using a natural coordinate system with one axis parallel to the mean direction of the precipitation features. In this coordinate system, the u-component was parallel to the direction of motion and the v-component orthogonal to this direction.

From the temperature and humidity data, vertical profiles of equivalent potential temperature over water and ice (θ_e and θ_{ei}) were calculated. Since all the cases studied occurred in the winter, it was felt that the ice process was important. The equations and assumptions used in these calculations are discussed in Appendix III.

Because of the assumptions necessary to compute these variables, and the poor spatial and temporal resolution of the ascents, only a qualitative picture of the vertical structure of the atmosphere, during the times the mesoscale precipitation features were evolving, was obtained.

The height of the steering level and the magnitude of the u-component of the wind at this level were determined from the vertical wind profiles. The steering level was defined as the level where the v-component of the wind approaches zero and

changes sign while the u-component of the wind remains positive. If this occurs over a deep layer, the center of this layer is defined as the steering level. The heights of any temperature inversions or convectively unstable layers were also determined using both the θ_{ei} and wind vertical profiles. From the positions of these layers with respect to the steering level and the RHI-derived vertical structure, the layer within which the observed mesoscale precipitation features were moving was determined. The nature of the three-dimensional structure of the atmosphere during the times of the mesoscale precipitaion features was compared with the structures described by Browning and Harrold (1973), Harrold (1973), and Kreitzberg and Brown (1970).

5. Precipitation amounts

The hourly precipitation amounts for seventeen stations in New England were plotted in histograms to show the variations in surface rainfalls as the observed mesoscale precipitation features passed over a fixed point. The seventeen stations were chosen as representative of either different regions of the CsF circulation or regions with different orographic characteristics (i.e. hills vs. plain). The stations and the areas they represent are listed in Table 2. Their locations and the area covered by the radar are shown in Figure 1.

For these seventeen stations, the mean total precipitation amount, the mean amount of precipitation during the time the CsF was present, and the mean amount of precipitation associated with

the specific mesoscale precipitation features observed by radar were computed. To calculate the enhancement, if any, caused by the CsF circulation, the precipitation, associated with the mesoscale features that fell west of the CsF zone was compared to that which fell in the CsF zone. The amount of enhancement is the precentage increase of the amount in the CsF zone over the amount west of the CsF zone.

To calculate the enhancement from orographic effects, a similar process is performed using the mean amounts of precipitation from the mesoscale features for the stations in the hills versus the stations on the plain east of the hills. The amount of enhancement, if any, is the percentage increase of the amount in the hills over the amount for the plain. Comparison of the tendency for enhancement in these two different areas was made in an attempt to ascertain whether the enhancement observed by Bosart was due to orographic effects or to some mechanism related to the CsF circulation.

The hourly precipitation data for the two non-CsF situations were analyzed in a similar manner, comparisons being made for the same groups of stations, as if a CsF were present. The resultant enhancement or suppression was then compared to that found for the CsF cases. Thus an estimate was made as to the significance of the enhancement due to the presence of the CsF.

III DESCRIPTION OF INDIVIDUAL CASES

A. Explanation of Tables

In this chapter one of the six cases will be described in detail, the other five in summary form. To facilitate comparisons tables were constructed, combining all the cases, for characteristics of each feature described. These tables are as follows: Table 3, the characteristics of the synoptic-scale cyclone; Table 4, the characteristics of the CsF; Table 5, the characteristics of the observed mesoscale precipitation features (i.e. LMSA's); Table 6, the characteristics of the vertical structure; Table 7, the characteristics of the overall precipitation pattern.

A typical structure in the vertical profiles of wind and θ_{ei} was encountered in every case. A schematic representation of this structure, which is described below, appears in Figure 2.

The surface layer consisted of cool dry (low θ_{ei}) air that was relatively neutral in stability (no vertical θ_{ei} gradient). The top of this layer was a strong inversion (sharp increase of θ_{ei} with height). The mean height of this inversion for the six cases was approximately 1.0 km.

Above the inversion was a layer of stable warm moist (higher θ_{ei}) air. The mean depth of this layer for all six cases was about 2.6 km. The air in this layer was almost always saturated with respect to ice and usually saturated with respect to water.

At the top of the moist layer was a relatively thin convectively unstable (θ_{ei} decreasing with height) layer, usually less than 1 km thick. The mean height of this layer was about 3.6 km.

Above the convectively unstable layer was a layer that was characterized by a neutral vertical θ_{ei} structure and weak vertical wind shear. The homogeneity of the vertical structure implied a very well mixed layer. It is assumed that the mixing was caused by convective overturning which resulted from the realization of convective instability due to previous lifting of the layer. Therefore, this layer is referred to as a convectively mixed layer.

The height at which the homogeneity gave way to relatively strong vertical θ_{ei} and wind shear again was defined at the top of the convectively mixed layer. This was assumed to be the upper limit of the cloud. The mean height of this level was approximately 6.2 km.

The steering level was always within or just below the convectively mixed layer. Its mean height was 4.6 km.

Also listed in the five tables described above, are the characteristics of the various features for the two non-CsF cases taken from Reed (1972).

B. Case Analysis: 8 December 1969

1. Characteristics of the synoptic-scale cyclone

The principal cyclone for this case was a weak wave that developed along the Norht Carolina coast at 03Z. It moved northeastward, filling slowly, at 7 m sec^{-1} and passed over Boston at 09Z, 9 December 1969, as indicated in figure 3a. Figure 3b depicts the section of the cyclone that was observed by the radar.

2. Coastal front characteristics

The CsF developed at 06Z in the cold air 875 km ahead of the surface cyclone. Lasting 15 hours, the CsF reached its peak intensity at 15Z. An analysis fo the CsF position at this time appears in Figure 4.

At this time, the horizontal temperature gradient and wind shear, between BOS and ORH, are 0.7C per 10 km and cyclonic with a magnitude of 7 deg per 10 km, respectively. The vertical profiles of θ_{ei} and wind at PWM for 12Z indicated that the CsF was in the surface layer and had a height of 300 m.

The CsF finally lost its identity at 21Z as the surface cyclone approaced Boston.

3. Characteristics of the mesoscale precipitation patterns

Continuous radar coverage was available from 1300Z to 1630Z. From 1630Z to 1800Z there was a break in the data caused by an

incorrectly set elevation angle. Continuous data were again available from 18Z to 22Z.

The observed mesoscale precipitation pattern was characterized by three easily discernible bands moving from 240° at 18 m sec^{-1}. These bands first appeard while the surface cyclone was still 500 km to the southeast of Boston. Figure 5 depicts the tracks of these three bands.

The bands were approximately 90 km apart and between 25 km and 35 km wide at intensity level four, the first two bands being much narrower than the third. The tops of the echoes, taken from the RHI, for the first two bands were 6 km. For the third band the tops reached almost 11 km.

4. Characteristics of the vertical structure

The vertical profiles of θ_{ei} and wind for ALB at 12Z and PWM and ACK at 00Z, 9 December 1969, were computed. A listing of the features of the vertical structure is in Table 6.

The height of the inversion at the top of the surface layer gets lower from 12Z to 00Z as the surface cyclone approaches. At both times this inversion is relatively strong, with θ_{ei} differences across it from 284K to 295K at 12Z and from 291K to 303K at 00Z. This inversion definitely appears to be the base of a warm frontal zone.

As the surface cyclone approaches, the depth of the layer of stable warm moister air increases indicating a deeper layer of saturated air just above the frontal zone to support precipitation growth.

The convectively mixed layer was lower at 12Z, around the time the observed bands were just beginning, than it was at 00Z, after the bands had disappeared. The height of the steering level moved accordingly.

The speed of the wind at the steering level was in good agreement with the observed mean motion of the observed bands. Also, the top of the convectively mixed layer was in agreement with the RHI-derived echo tops.

5. Characteristics of the overall precipitation pattern

The average total precipitation for this storm was 29.0 mm over a period of 26 hours. Of this average amount, 11.7 mm fell during the 15 hours the CsF was present. The average amount of precipitation that fell from the bands was 9.9 mm, all while the CsF was present. The hourly distribution of precipitation at representative stations in each region investigated can be seen in Figure 6; Boston, in the CsF zone; East Brimfield Dam, west of the CsF zone; Surry Mountain Dam, in the hills; and Everett Dam, on the plain east of the hills. Table 7 lists the mean amounts, variances, and standard deviations for the

precipitation amounts, from the bands, in each region.

There is an observed enhancement of the precipitation in the CsF zone (average of 2.0 mm). While this enhancement is not large it exceeds the standard deviations in all the regions except that for the hills.

In the hills there is no clear enhancement of the precipitation. In fact it is negative and smaller than the standard deviation.

C. Synopsis of Other Five Cases

Analysis of the other five CsF cases listed in Table 1 indicated that with respect to the characteristics of the synoptic-scale cyclone, the CsF structure, and the vertical structure of the atmosphere, these cases were very similar to the one discussed above (see Tables 3,4, and 6). The characteristics of the mesoscale precipitation patterns and the related overall precipitation distribution for the five cases however did exhibit some important discrepancies and similarities.

The typical larger mesoscale precipitation features for all five cases, as in the one discussed above, were bands or lines of echoes. These bands however, were not always the main mesoscale precipitation features. In particular, this was true for the cases of 15 February 1970 and 24 December 1970.

The main mesoscale precipitation features for the case of 15 February 1970 were two that fell into the SMSA size

classification of Austin and Houze (1972).

These two SMSA's were moving parallel to and on the north side of what appeared to be a low-level jet. This jet appeared at 21Z; at that time the precipitation areas seemed to increase their translational speed to 33 m sec^{-1}. This also happened to be the time at which the CsF became indistinguishable from the mean geostrophic flow around the baroclinic disturbance. The jet was oriented on an axis of 247-157 degrees on a line between Portsmouth, New Hampshire and Springfield, Massachusetts. The SMSA's were elongated along the jet axis. The tracks of the SMSA's are shown in Figure 7. Figure 8 depicts the PPI tracing for 2245Z showing the orientation of the SMSA's along the jet axis.

The SMSA's associated with the jet affected the overall precipitation distribution by increasing the amount falling in the hilly terrain under the jet axis. This increase resulted in more overall precipitation falling in this region than in that affected by the CsF circulation. The differences can be seen in Table 7 and Figure 9.

For the case of 24 December 1970, the main mesoscale precipitation feature was an unusually persistent precipitation area centered over Boston, Massachusetts. This precipitation area formed in a region of the coast where the CsF was developing rapidly and did not move as the lines of precipitation did.

This mesoscale area was very weak in intensity, but was observed to persist on the radar until 03Z. It was elongated along a northwest to southeast axis and was approximately 40 km long and 25 km wide. As each line of echoes passed through this small mesoscale area the area became elongated along the axis of the line. Figure 10 is a PPI tracing of this area at 0030 Z. Because this echo is in the region of radar ground clutter, the intensity cannot be adequately determined. Therefore only the outline at the lowest intensity level is shown.

The height of the small mesoscale area, as seen in RHI cross-section at 0100 Z (Figure 11) is between two and four kilometers.

The small mesoscale area was the dominant cause for the extremely large difference in the precipitation between the area in the CsF zone and that west of the CsF zone. Also, it was the dominant cause for the large variance within the CsF zone. These differences can be seen in Table 7. Figure 12 shows the hourly precipitation distribution in the different regions for this case.

Except for the precipitation in the vicinity of the jet on 15 February 1970 and the SMSA on the 24 December 1970, every case exhibited similarity in their precipitation patterns. A series of bands, usually two or three, passed over the region

and the precipitation in the vicinity of the CsF would exceed that in the region to the west. The percent of enhancement varied from near 0 to 196 but was always positive (see Table 7).

This was not the case for the precipitation falling from the bands in the hills or on the plains east of the hills. In these regions there was no consistent pattern of enhancement.

The observed enhancement was obtained from the hourly rainguage data because of the difficulty in detecting small differences in precipitation rate from the PPI films. The factor of two increases in rainfall rate encountered when the intensity level is increased makes it difficult to detect the enhancement in the CsF zone with radar. Only in the extreme case (24 December 1970), where the enhancement was of the order of a factor of two increase, could the enhancement be detected on the radar data.

IV. Discussion

A. The Coastal Front

In each case the CsF developed in the cold air, at least 500 km ahead of the surface cyclone center, along the southeastern coast of New England. This development was clearly independant of the large scale baroclinic disturbance represented by the surface cyclone.

All six CsFs formed on a line between Boston, Massachusetts and Providence, Rhode Island with a tendency to extend as far north as the central Maine coast. The northern extent of the CsF was hard to determine with surface data available only from Portland, Maine along the coast in this region.

The average duration of the CsF was 12 hours, with a maximum of 15 hours and a minimum of 7 hours. At peak intensity it was characterized by a strong horizontal temperature gradient and cyclonic wind shear. The average horizontal temperature gradient was 3.0 C per 10 km. The horizontal wind shear was always cyclonic, the average magnitude being 14.0 deg. per 10 km, and the maximum 28.0 deg per 10 km.

The vertical extent of the CsF, for all cases studied confirmed Bosart's result that it was a separate entity from the main synoptic-scale warm front. The mean height of the CsF for all the cases was 300 m, while the mean height of the inversion

at the top of the surface layer usually the base of the warm frontal zone was 1.0 km.

B. Mesoscale Precipitation Features

The observed larger mesoscale precipitation features in all the cases were band-shaped and had a size scale near the upper limit of the LMSA scale (i.e. 10^4 km^2) defined by Austin and Houze (1972). The mean width of these bands was approximately 30 km, with a range of 20 km to 40 km. The mean distance between bands was approximately 90 km, with a range of 60 km to 130 km.

The lengths of the bands were hard to determine because of the possibility of their extending beyond the range of the radar, but for some cases a rough approximation to the length to these bands could be made by checking the hourly rainfall amounts for statrons just outside of the radar range. Most of the larger bands had lengths of at least 150 km, while some of the smaller bands were closer to 100 km in length.

The observed values of the spatial distribution and dimensions of these land-shaped features are very consistent with those obtained by Elliot and Hovind (1964) for convective bands in an occluded cyclone along the west coast of the United States. They are also consistent with the values obtained for the bands discussed by Browning, et. al. (1973) and Harrold (1973).

The spatial distribution and motion of these precipitation

bands indicated that they were associated with the large-scale baroclinic circulation rather than the local CsF circulation.

It must also be noted that in two cases the bands were not the principal mesoscale precipitation features as far as the overall precipitation distribution is concerned. On 15 February 1970, two small mesoscale areas moving parallel to a low-level jet were of main importance to the overall precipitation distribution. On 24 December 1970, a SMSA over Boston, associated with the initial development of the CsF, was most important to the distribution of precipitation.

C. Vertical Structure

The typical vertical structure of the atmosphere during the times the observed bands were present, as outlined in the last chapter (i.e. Figure 2), was consistent with that observed by Kreitzberg and Brown (1970), Harrold (1973), and Brown, et. al. (1973) in extra-tropical cyclones. A summary of the vertical structure for all the CsF cases studied plus the two non-CsF cases appears in Table 6.

The key feature of the vertical structure is the convectively mixed layer. It is formed as a result of the realization of convective instability through some means of lifting this layer. The convective instability is a result of a flow of cold dry (low θ_{ei}) mid-tropospheric air over a layer of warm moister

(higher θ_{ei}) air. The observed bands represented lines of convective activity that formed when enough lifting caused the layer of warm moister (usually saturated) air to become unstable. The fact that the steering level for these bands is typically embedded in the mixed layer supports this contention.

The lifting necessary to cause the mixed layer to develop has been proposed, by Kreitzberg and Brown (1970), Harrold (1973), and Browning, et.al. (1973), to come from the broad synoptic-scale vertical velocity that occurs as a result of the baroclinic process within a cyclone. This type of lifting, while explaining the release of convective instability, does not explain why the precipitation areas form in bands or lines. Some hypotheses have been proposed to explain the line structures, but will not be discussed here since they are not relevant to the role of the CsF.

The tops of the convectively mixed layer, as determined by the method outlined in the previous chapter, appeared to be in good agreement with the cell tops observed on the RHI. The only exceptions were the cases with alot of snow, probably because of the poor detectability of snow by radar.

Another interesting feature of the typical vertical structure is the layer of stable warm moist air just below the convectively mixed layer. This layer, usually saturated, appears to be comparable to the "conveyor belt" of Harrold (1973) and Browning, et. al. (1973).

The layer of saturated air was probably the source of moisture for the convective bands as well as a layer that would support the growth of hydrometeors falling through it.

The inversion at the base of the warm moist stable layer, in some cases, was clearly the base of the warm frontal zone extending ahead of the surface baroclinic disturbance.

D. Overall Precipitation Pattern

In practically every CsF case studied, most of the total precipitation fell during the time the CsF was present. In all eight cases, with and without the CsF, the total amount of precipitation features (i.e. bands and SMSA's).

In agreement with Bosart's findings, practically every CsF case had an enhancement of the precipitation falling from the observed bands in the CsF zone. This enhancement, although not statistically significant, was consistently positive in this zone.

In the two cases without a CsF taken from Reed (1972) there was no clearly established enhancement of the precipitation in a region along the southeastern coast of New England. One did show slight enhancement, but it was smaller than the standard deviations on the various regions. The other showed a diminution of precipitation in the CsF zone.

In the hills there was no clear pattern of enhancement or diminution of the precipitation falling from the observed bands.

Comparing this result to the consistent positive enhancement found in the CsF zone clearly supports the conclusion that the CsF is the mechanism causing the enhancement in this zone rather than some type of orographic effect.

These results imply that the majority of the precipitation in the CsF cases is associated with the bands and falls while the CsF is present. Therefore, for there to be an enhancement of the overall precipitation distribution in the region of the CsF, as described by Bosart, there must be some form of constructive interaction between the low level CsF circulation and the precipitation falling from the observed bands.

E. Interaction Between the Coastal Front and the Observed Bands.

As was stated previously, the height of the warm frontal inversion, during the time the CsF was present, was clearly above and separate from the CsF inversion. This type of structure indicates that the CsF, in the surface layer, and the observed bands, whose precipitation developed above this strong inversion in the convectively mixed layer, were separate entities. The CsF would form locally, independent of the baroclinic disturbance to the south, while the bands were directly dependent on the large scale baroclinically induced circulation. Consequently, for there to be an interaction between the two circulations to enhance the precipitation falling in the bands, it must occur in the surface

layer below the warm frontal inversion. The most likely form of this interaction is an increase in the liquid water content through a convergence of water vapor by the CsF circulation. This in turn could supply a source of water for increased low level growth of the hydrometeors (snow, in these cases) falling in the bands from above this layer.

The question might be raised as to whether the observed amounts of enhancement are consistent with condensation in such a shallow layer and accretion of the droplets by falling snowflakes. Some estimates of the water vapor convergence and cloud water content required for the extreme Case, 24 December 1970, suggest that the hypothesis is reasonable. In this case the mean precipitation rate for 15 hours outside the CsF zone was 0.46 mm hr^{-1} while in the CsF region it was 1.36 mm hr^{-1}.

The mean surface two-dimensional water vapor divergence or flux ($\nabla \cdot r\underline{V}$) was present. The details of this computation appear in Appendix IV and Figure 13 depicts the mean divergence field.

Comparison of this mean divergence field with the position of the CsF at 00Z (see figure 14) indicates that the strongest convergence of water vapor occurs just on the warm side of the CsF zone. The mean value of this convergence is 3×10^{-4} g m^{-3} sec^{-1} or an influx of water vapor into the CsF zone of approximately 1.0 g m^{-3} hr^{-1}. This maximum occurs at the surface

where the horizontal temperature and wind gradients are the strongest.

The maximum convergence is along the CsF surface which slopes toward the cold air with height. When the frontal surface becomes horizontal the horizontal gradients disappear and consequently so does the convergence. If the zone of maximum convergence is assumed to extend up along the frontal zone, as shown in Figure 15, a rather deep layer of cloud would probably develop over the cold air side of the surface CsF position from the convergence-induced lifting. If it is assumed that the water vapor convergence extends up to 600 m with a mean value of 1.5×10^{-4} g m^{-3} sec^{-1} in that layer (see Figure 15), and that all of the converged water vapor falls out as precipitation, an increase of 0.35 mm hr^{-1} in the existing precipitation rate would occur. This increase is less than the 0.90 mm hr^{-1} increase that is observed, but is of the correct order of magnitude.

A simple calculation was made to determine the depth and mean liquid water content of the cloud necessary to produce the desired enhancement for this particular case. This calculation was performed assuming a constant size distribution of aggregated snowflakes, representing a precipitation rate of 0.46 mm hr^{-1}, falling into the surface layer from above the warm frontal inversion. These aggregates were assumed to fall through a cloud in the surface layer and to grow by collection of cloud droplets. By varying the

depth and mean liquid water content of the cloud, a range of combinations of the two variables that would produce the observed enhancement was computed. Figure 16. shows combinations of the two variables that will give the observed enhancement in the CsF zone of 0.9 mm hr^{-1}. The details of these computations appear in Appendix V.

Inspection of Figure 16 indicates for this particular case it would be very easy to acheive the enhancement with reasonable values of cloud depth and mean liquid water content especially considering the large values of water vapor convergence into this region.

These results support the hypothesis that the enhancement in the CsF cases is produced by an increase in the low level water content due to convergence and lifting of water vapor by the CsF circulation. The CsF circulation would tend to increase the liquid water content above the cold air just west of the CsF surface position. The accretion of this (increased low level) moisture by hydrometeors falling in the observed bands from above the surface layer produces the enhancement of precipitation on this side of the CsF zone.

An attempt to find further support for this hypothesis was made by checking the hourly surface reports of visibility, ceiling, and wind at BOS and ORH for the extreme case (34 December, 1970) during the times the CsF was present (see Table 8). Both stations were in the cold air west of the CsF zone until 04Z. Between 03Z

and 04Z the wind at Boston shifted form northerly to easterly as the CsF moved by. Prior to this the ceiling at both stations was low, estimated around 60 -120 m. After the wind shift at Boston the ceiling was higher, rising to 210 - 270 m, while at Worcester it remained near 60 m. These observations seem to fit nicely with the schematic representation of hte enhancement mechanism in Figure 15.

F. Forecasting Considerations.

The preceding discussion points up the large variations in precipitation amounts that are encountered in a typical CsF situation. The number of variables that interact to acheive the overall effect is large and their interactions complex. It would be very difficult for a forecaster to consider all of the variables for each possible CsF situation and still get a forecast out. However some simple guidelines based on Bosart's results and those of this study may be useful.

First, one must determine when and where a CsF will develop. The CsF is primarily a late fall, early winter phenomenon that develops when a mean surface geostrophic easterly flow prevails over New England. It has a tendency to develop along a line from Boston, Massachusetts to Providence, Rhode Island.

After it has been determined that a CsF is likely to develop then the probability of an enhancement of precipitation is greater. Any enhancement which occurs will be near the CsF zone especially

on the cold-air side of the surface CsF position. The enhancement process will start as soon as there is enough moisture converged to produce condensation for low cloud development. These low clouds will either produce enough condensed water to precipitate by themselves or will add moisture to hyrometeors falling from above. The amount of overall enhancement is more difficult to predict and most likely will be dependent on the strength of the CsF circulation and the availability of water vapor.

There few guidelines may not seem highly analytic, but if they can help alert forecasters to the possible development of a CsF situation and its subsequent affect on the overall precipitation distribution that would be a step in the right direction.

V. Summary and Suggestions for Further Study

A. Summary

Characteristics of the precipitation were studied for six storms where mesoscale coastal front developed in eastern New England. In all six cases, the principal larger mesoscale precipitation features were band-shaped. These bands were associated with the large-scale baroclinically-induced circulation. Typically, the precipitation falling in these bands developed in convective clouds embedded in a layer of cold dry mid-tropospheric air. These convective clouds had their "roots" in a layer of warm saturated air just below this mid-tropospheric layer.

The CsF, in all six cases, developed locally in the cold surface layer. Its development was independent of the large scale baroclinically induced circulation.

The overall precipitation pattern indicated that there was within the CsF zone enhancement of the precipiation falling in the observed bands. Typical values of the enhancement were on the order of 20-30 percent, with a range extending from near 0 percent to 169 percent. This enhancement, although it may not be statistically significant, was present in every case which was studied.

The mechanism which caused the enhancement was hpothesized to be low-level growth of hydrometeors. The low-level growth would be supported by convergence of water vapor by the coastal front circulation in the surface layer near the coastal front. Results of computations of the observed surface water vapor convergence and of cloud depths and liquid water contents necessary to produce the observed enhancement indicate that this hypothesis is a reasonable one.

Although the coastal front enhancement appeared in every case it was not always the principal mechanism affecting the overall precipitation distribution. In one case another mesoscale feature, a low-level jet, was the principal mechanism affecting the precipitation distribution.

B. Suggestions for Further Study.

Further study should be directed toward both observational and theoretical attacks on the problem of understanding the effect which the CsF, as well as other mesoscale mechanisms (i.e. low level jets and orography), have on the distribution of precipitation from a given storm. An observational attack on the problem could be accomplished realistically through a co-ordinated effort to measure the necessary parameters in these types of situations. Incorporated in such an investigation would be the use of digital radar data and high resolution

ranging and upper air data.

Digital radar data, available in the near future at M.I.T., will be helpful in quantitative rainfall studies of this type, where small changes on rainfall rate are important, because of the higher resolution of reflectivity data. Rather than being in intensity level steps of 4-5 db as in the PPI films, these data will have intervals of only 1 db. It will make possible more efficient data processing, especially time integrations to obtain total rainfall amounts.

High resolution raingauge data, available from a number of stations in New England, would act as the ground truth for the radar data and would also provide information on the amount of precipitation, falling at rainfall rates too low to be detected by radar.

Rawindsonde ascents are routinely made every 12 hours at the four stations used in this study. By increasing the frequency of these ascents to 2-3 every 12 hours, better resolution of the three-dimensional structure of the atmosphere could be obtained during the times observed mesoscale features (i.e. CsF, low-level jet, bands, etc.) are present.

On the theoretical side, investigations into the mechanisms determining the configuration of mesoscale features in extra-tropical cyclones are strongly recommended. Of particular interest

is the fact that they are band-shaped. Several papers have been published (Einand: and Lalas, 1975 and Matsumoto and Ninomiya, 1969) in which this problem is addressed using the hypothesis that these bands are wave-induced, on the size scale of gravity waves. It is hoped that the spatial distributions and atmospheric vertical structure reported in this study will provide further insight to such investigations.

Finally refinement of the theory for the CsF mechanism requires further detailed observations of the circulation of this phenomenon.

Type A: 17 cases

These cases were associated with the passage of an intensifying cyclonic disturbance up the Atlantic seaboard. A cold anticyclone was situated north of New England.

Type B: 25 cases

These cases differed from those of type A in that a primary cyclone moved toward the Great Lakes while a secondary developed south of New England.

Type C: 3 cases

These cases, while relatively rare, were similar to type B with the major-exception that the secondary evolution was noticeably absent. Additionally, the cold anticyclone was quite strong

(in excess of 1030 mb) such that a strong southerly geostrophic flow was established across New England.

Type D: 4 cases

These cases were similar to type A with two major exceptions: (1) little intensification was observed in the cyclone, and (2) the cyclone lached a well defined center and was elongated northeast-southwest over several hundred kilometers. A weak anticyclone was over Canada.

Type E: 8 cases

These cases were characterized by an east-west frontal zone south of New England along which weak waves moved. Similarly, an anticyclone extended east-west across southeastern Canada.

Table 1

New England Coastal Front Cases

Date	Synoptic Type	CsF
12/8/69*	B	yes
2/15/70	B	yes
12/23-24/70	B	yes
1/14/71	B	yes
2/5/71	B	yes
12/30/71*	B	yes
11/14/69*	-	no
12/11/69*	-	no

*Cases also covered in Reed (1972).

Table 2.

Stations Used for Precipitation Characteristics

West of the CsF Zone	In CsF Zone
Hudson, N.H.	Boston, Mass.
Worcester, Mass.	Blue Hill, Mass.
East Brimfield, Mass.	Providence, R.I.
Hartford, Conn.	Block Island, R.I.
Mansfield Hollow Dam, Conn.	or
Jewitt City, Conn.	New Bedford, Mass.

East of CsF Zone	East of the Hills
Hyannis, Mass.	Hopkington Dam, N.H.
or	Concord, N.H.
Provincetown, Mass.	Everett Dam, N.H.
	Hudson, N.H.
In the Hills	Worcester, Mass.
Surry Mountain Dam, N.H.	
Winchester, N.H.	
Birch Hill Dam, Mass.	

Table 3.

Characteristics of the Synoptic-Scale Cyclone

	12/8/69	2/15/70	12/24/70	1/14/71	2/5/71	12/30/71	11/14/69	12/11/69
Intensity trend	filling slowly	deepening slowly	deepening	deepening	deepening slowly	deepening slowing	filling slowly	deepening
Distance from BOS when CsF appeared (km)	875	550	660	985	740	515	-	-
Distance from BOS when first lines appeared (km)	500	390	320	381	490	-	525	500
Mean motion* (deg. from/ m/sec)	246/05	230/16	230/12	240/12	245/17	262/19	190/10	190/17

*during the times the lines or bands were observed.

Table 4.

Characteristics of the Coastal Front

	12/8/70	2/15/70	12/24/70	1/14/71	2/5/71	12/30/71	Mean
Time CsF present (Z)	06-21	09-21	21(12/23) -12	12-21	06-21	17- 00(12/31)	-
Duration (hrs)	15	12	15	9	15	7	12
Time of max. strength (Z)	15	16	09	17	15	18	-
Max. hor. temp. grad. (°C/10 km)	1.3	4.0	7.6	1.8	1.5	2.0	3.0
Max. hor.* wind shear (deg./10 km)	7	28	20	11	13	4	14
Station used to compute gradients	BOS-ORH	BOS-BED	BOS-BED	PVD-EWB	CON-PSM	BOS-BED	
Depth of CsF(m)	300 (12Z)	400 (12Z)	350 (00Z)	300 (12Z)	200 (12Z)	300 (00Z)	300

*positive indicates cyclonic shear.

Table 5.

Characteristics of Mesoscale Precipitation Areas

	12/8/69	2/15/70	12/24/70	1/14/71	2/5/71	12/30/71	11/14/69	12/11/69
Times radar data available (Z)	13-1630; 18-22	17-2315	2120(12/23)-0130; 08-1144	1810-1930	1415-1726;21-0015(2/6)	14-2130	13-22	0530-1530
No. of lines or bands	3	3	3; 2	1	2; 1 main	6	4	3
Direction of movement (deg. from)	245-235	243	252;242	268	252	248-265	188	206
Speed (m/sec)	18	21	26;24	33	25;22	22-33	22	24
Width of bands or lines (km)	28	30	22;35	30	main-35 small-20	main-40 small-25	40	35
Distance between lines or bands (km)	90	80	90;75	-	main-110 small-75	main-130 small-75	70	90
RHI-derived tops (km)	max-11 mean-6	4 jet-7	4.5-5.5	-	3;3.5	5	5.5	6.5

Table 6.

Characteristics of the Vertical Structure

	12/8/69		2/15/70		12/24/70		1/14/71	2/5/71		12/30/71	11/14/69	12/11/69
Time (Z)	12	00	12	00	00	12	12	12	00	00	12	00
Stations profiles computed for	ALB	PWM* ACK	PWM ACK ALB JFK	PWM ACK	CHH ALB JFK	PWM CHH	PWM CHH ALB JFK	PWM CHH ALB JFK	PWM CHH	PWM CHH	PWM* ACK ALB	ALB*
Inversion height (km)	1.0	0.6	1.1	0.5	1.1	0.9	1.0	1.2	0.7	1.4	1.6	0.6
Base of convectively mixed layer (km)	2.3	3.9	4.0	4.2	3.7	4.0	2.9	3.9	3.0	3.6	2.9	2.1
Steering level (km)	4.0	4.7	3.6	6.5	3.8	5.2	3.2	4.3	5.7	4.6	2.5	6.5
Speed at steering level (m/sec)	18.5	14.5	23	41 jet	23	24	27	20	30	36	17	30
Top of convectively mixed layer (km)	9.0	6.2	5.6	7.2	5.2	6.5	6.2	4.8	5.2	5.8	5.5	5.9

Table 6 (con't.)

	12/8/69	2/15/70	12/24/70	1/14/71	2/5/71	12/30/71	11/14/69	12/11/69
Depth of warm moister air (km)	1.3 3.3	2.8 3.7	2.6 3.0	1.9	2.8 2.2	2.2	1.2	1.5

*no JFK soundings available on these dates

Table 7.

Characteristics of the Overall Precipitation Pattern

	12/8/69	2/15/70	12/24/70	1/14/71	2/5/71	12/30/71	11/14/69	12/11/69
Mean total precip. (mm)	29.0	11.7	17.0	5.6	19.3	18.8	11.2	36.6
Mean duration (hrs)	26	17	20	11	16	15	7	18
Mean amount of precip. associated with CsF times (mm)	11.7	7.4	12.9	4.1	17.8	14.2	-	-
Mean amount of precip. associated with observed bands (mm)	9.9	6.4	13.2	1.0	15.5	14.4	11.2	22.6
Mean amount in CsF zone (mm)	11.7	6.4	20.4	1.0 (5.3)*	20.6	15.7	13.7	18.3
Variance of amounts in CsF zone (mm^2)	0.59	7.81	58.06	0.06	5.22	2.32	5.08	7.62

Table 7 (con't.)

	12/8/69	2/15/70	12/24/70	1/14/71	2/5/71	12/30/71	11/14/69	12/11/69
Standard deviation of amounts in CsF zone(mm)	0.8	2.8	7.6	0.2	2.3	1.5	2.2	2.8
Mean amount west of the CsF zone (mm)	9.7	5.8	6.9	1.0 (4.1)*	15.2	14.7	10.7	29.7
Variance(mm^2)	2.32	3.16	2.32	0.26	1.61	6.45	8.38	18.54
Standard deviation(mm)	1.5	1.8	1.5	0.5	1.3	2.5	2.9	4.3
Amount enhancement in CsF zone (mm)	2.0	0.5	13.4	0.0 (1.3)*	5.3	1.0	2.0	-11.4
Percent enhancement	21	09	196	00 (32)*	35	07	19	-38
Mean amount in the hills (mm)	8.4	9.1	13.2	0.5	10.7	12.7	10.4	15.2
Variance(mm^2)	0.18	0.00	2.39	0.0	0.03	0.20	2.54	3.30

Table 7 (con't.)

	12/8/69	2/15/70	12/24/70	1/14/71	2/5/71	12/31/71	11/14/69	12/11/69
Mean amount east of the hills (mm)	9.9	6.6	10.4	0.5	14.9	13.4	11.7	24.1
Variance (mm^2)	3.16	3.16	40.32	0.06	10.9	6.45	3.30	35.56
Standard deviation (mm)	1.8	1.8	6.4	0.2	3.3	2.5	1.8	6.0
Amount enhancement in hills (mm)	-1.5	2.5	2.8	0.0	-4.3	-0.8	-1.3	-8.9
Percent enhancement	-15	38	27	00	-29	-06	-11	-37

*Amounts for all precipitation falling during the time the CsF is present.

Table 8.

Ceiling, Wind, and Visibility for BOS and ORH,

23-24 December 1970

	ORH			BOS		
Time (Z)	Ceiling (m)	Wind (deg)	Vis (km)	Ceiling (m)	Wind (deg)	Vis (km)
21	60	050	2.0	150	330	0.5
22	60	040	1.0	120	340	0.5
23	60	030	1.0	120	340	0.5
00	60	010	1.5	120	340	0.5
01	-	-	-	120	340	1.0
02	-	-	2.0	-	340	1.0
03	60	-	2.0	120	320	1.0
04	60	-	2.0	210	080	2.0
05	60	-	2.0	150	080	5.0
06	60	060	2.0	210	080	8.0
07	-	-	-	210	090	8.0
08	-	-	-	270	100	8.0
09	-	-	-	210	090	8.0
10	30	060	1.0	150	090	4.0
11	150	030	3.0	180	100	4.0

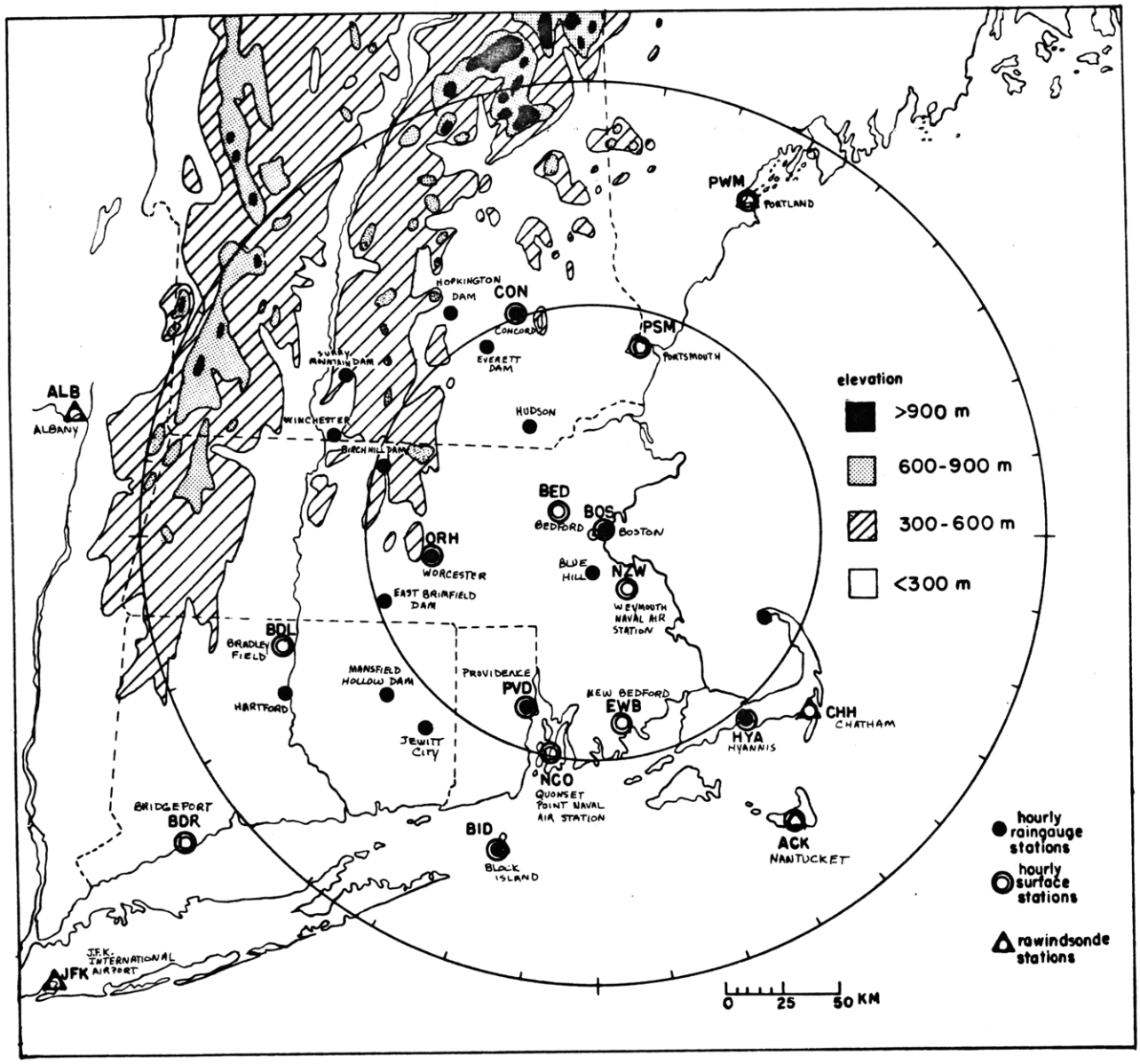

FIGURE 1: Station distribution and orographic features. The outer circle represents the extent of the radar coverage (200 km) and the inner circle is at a radius of 100 km.

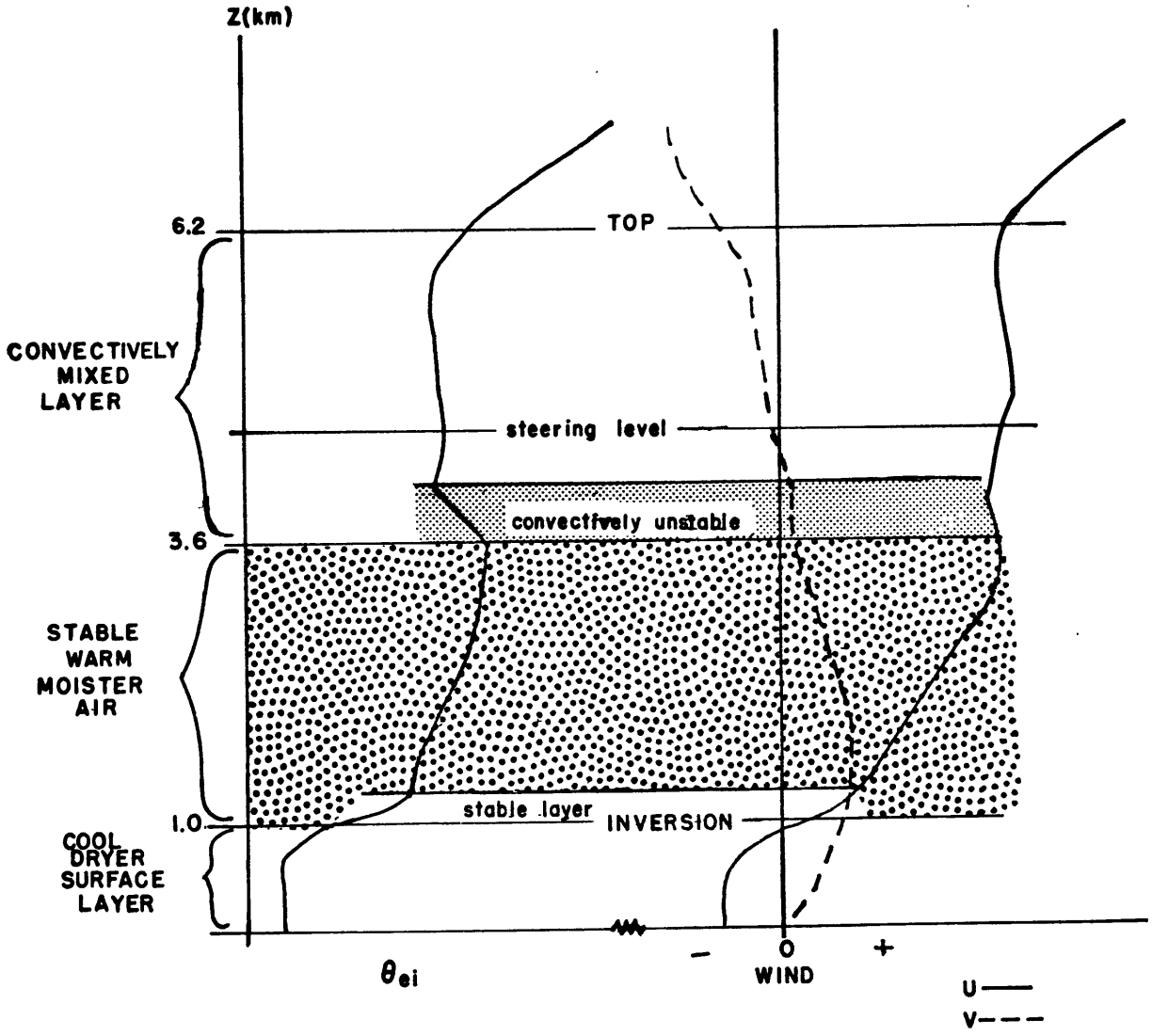

FIGURE 2: Typical vertical structure. The θ_{ei} profile is on the left and the wind component profiles are on the right.

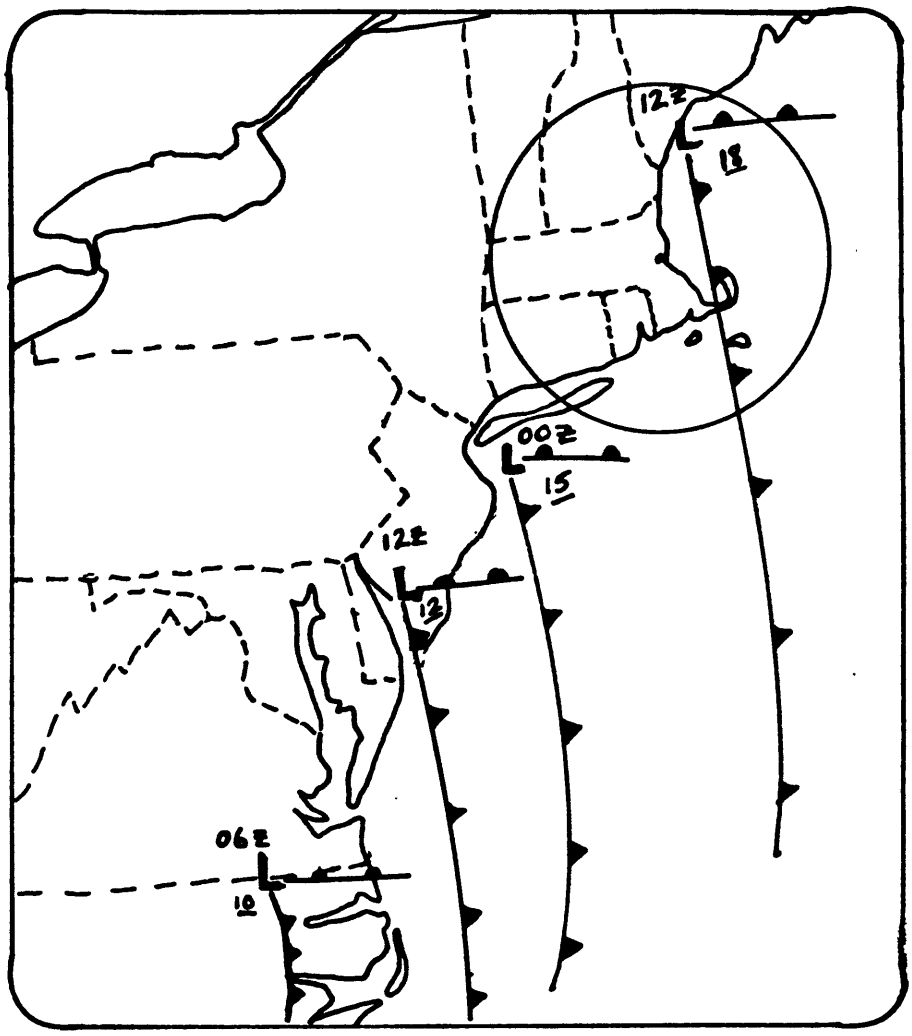

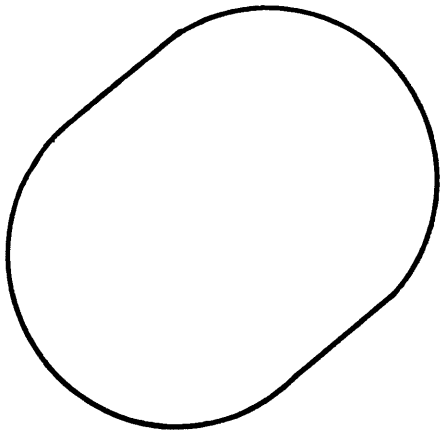

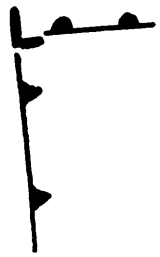

FIGURE 3: (a) Cyclone track and (b) the area covered by the radar for the case of 8 December 1969. Circle in (a) is 200 km in radius.

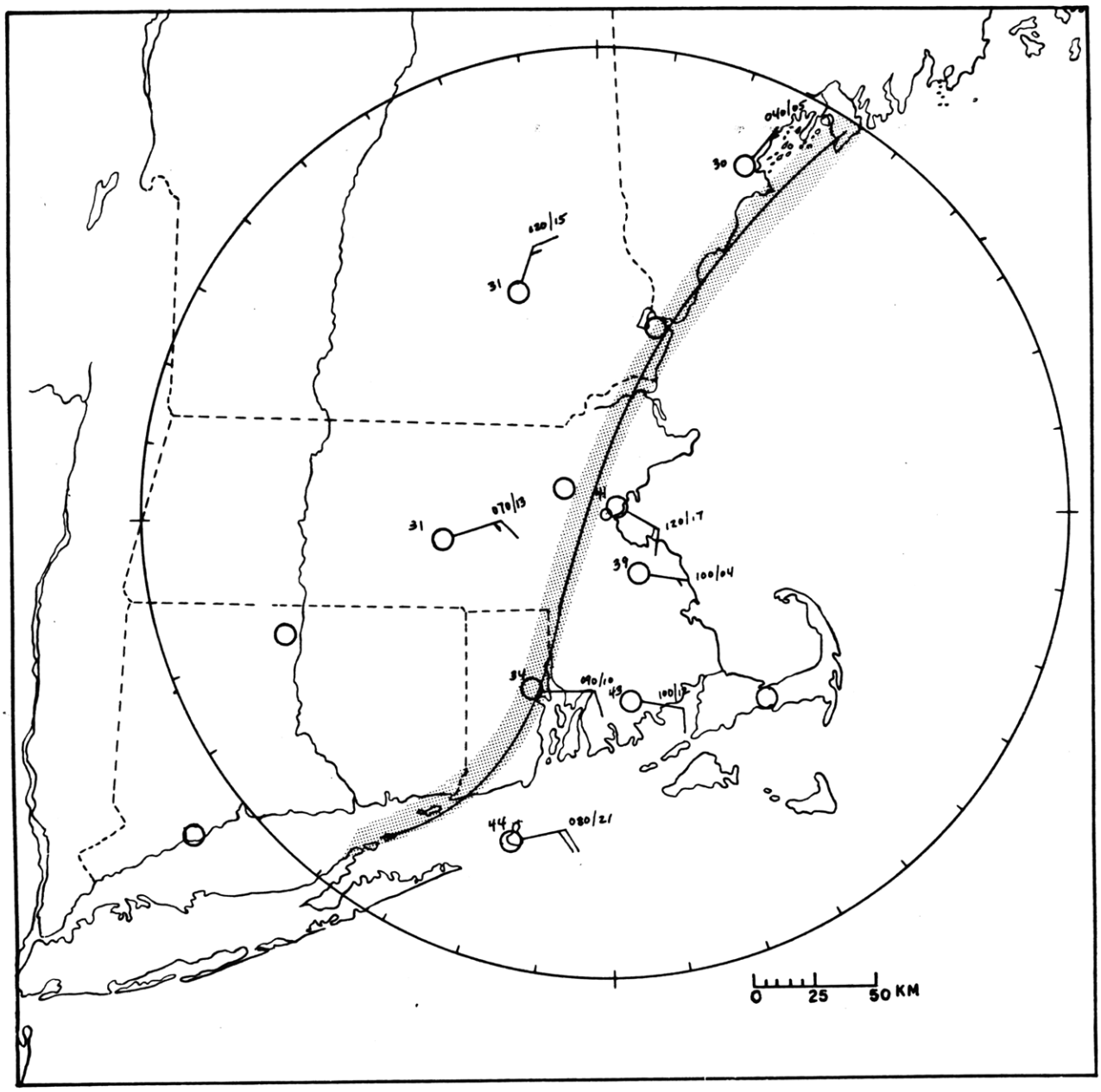

FIGURE 4: The CsF position at 15Z, 8 December 1969. The stippled area represents the approximate extent of the CsF zone. The station model shows the surface temperature (^{o}F) in the upper left and the wind is plotted and labeled in the standard format; direction in degrees and speed in knots.

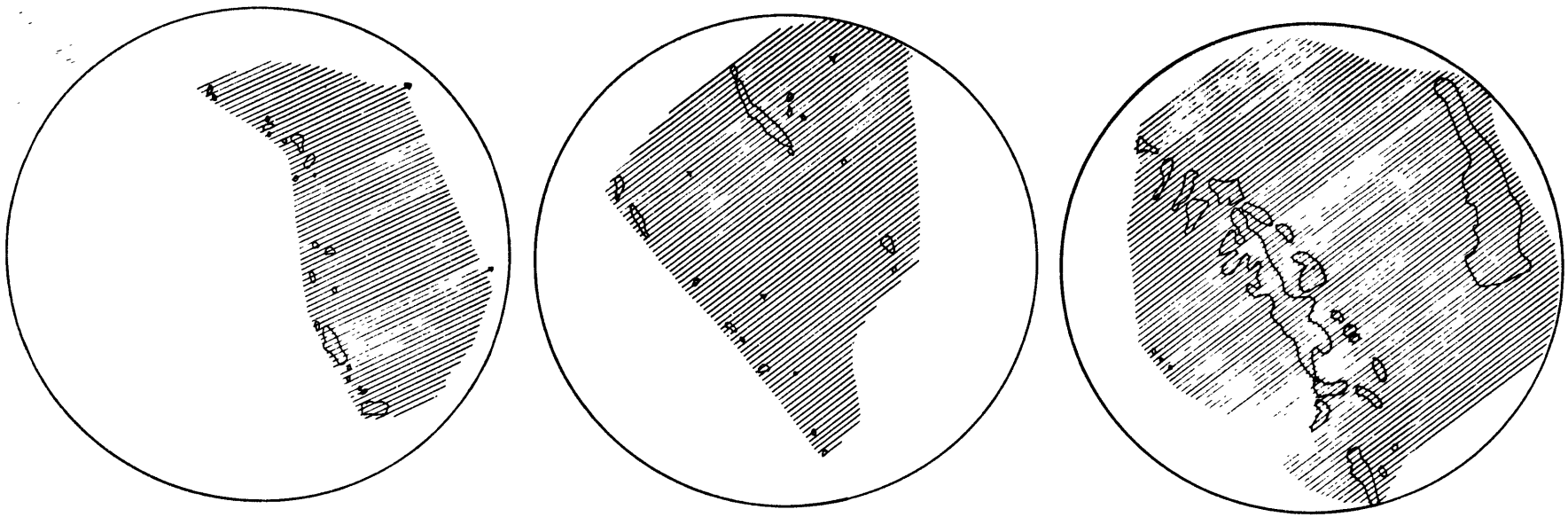

FIGURE 5: Tracks of the mesoscale precipitation features (bands) for the case of 8 December 1969 shown at intensity level four (~5mm hr^{-1} in rain). The circle is 200 km in radius and the lines indicate direction of motion. (a) The first band shown at 13Z; (b) the second band shown at 13Z and 15Z; (c) the third band shown at 15Z and 18Z.

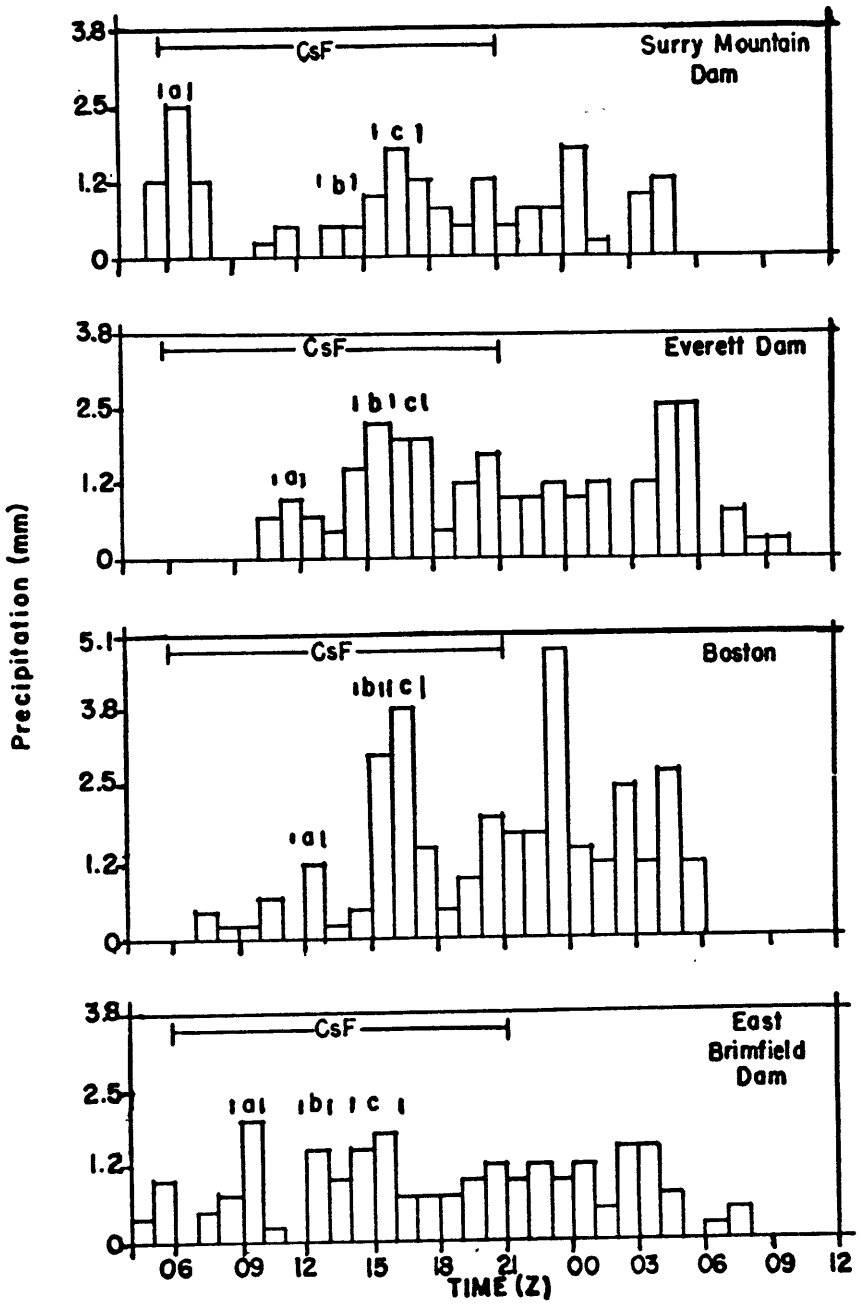

FIGURE 6: The hourly precipitation distribution for representative stations in the four regions investigated (see Table 2), 8 December 1969. The abscissa is time (Z) and the ordinate is precipitation (mm). The times that the CsF and the three labeled bands (a,b,c) were present are indicated by brackets.

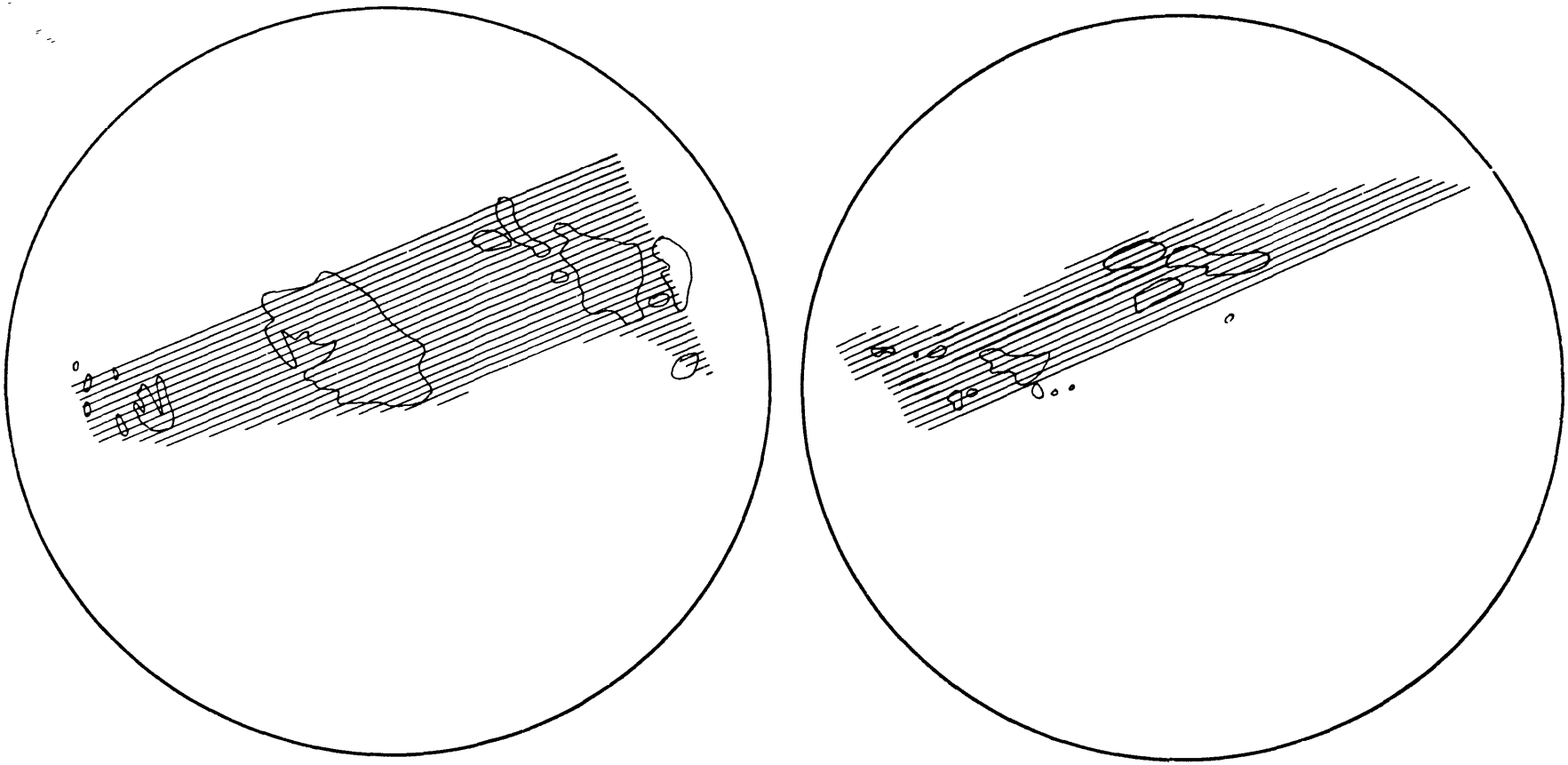

FIGURE 7: Tracks of the two SMSA's associated with the low-level jet, 15 February 1970, is shown at intensity level five (2mm hr^{-1} in snow). The circle has a radius of 200 km and the lines show the direction of motion. (a) The first SMSA shown at 21Z, 22Z and 23Z; (b) the second SMSA shown at 22Z and 23Z.

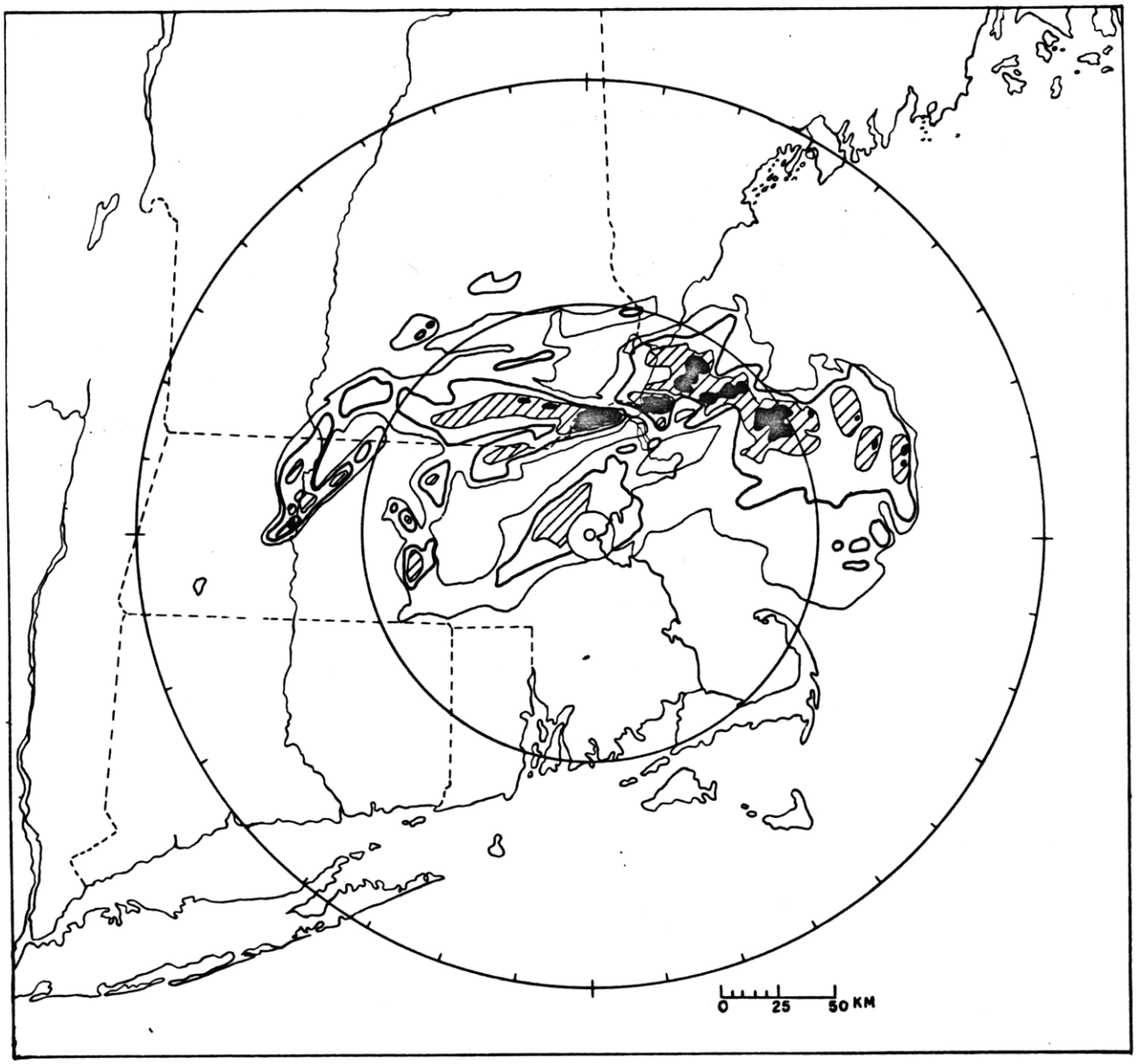

FIGURE 8: PPI tracing of the SMSA's, associated with the low-level jet, at 2245Z, 15 February 1970. The outer circle is 200 km in radius, the middle circle at 100 km radius, and the innermost one at approximately 10 km showing the ground clutter extent. The light solid line indicates the threshold of intensity level 3 (~0.5mm hr^{-1} in snow), the heavy solid line level 4 (~1mm hr^{-1} in snow), the cross-hatched area level 5 (~2mm hr^{-1} in snow), and the solid area level 6 (~3mm hr^{-1} in snow).

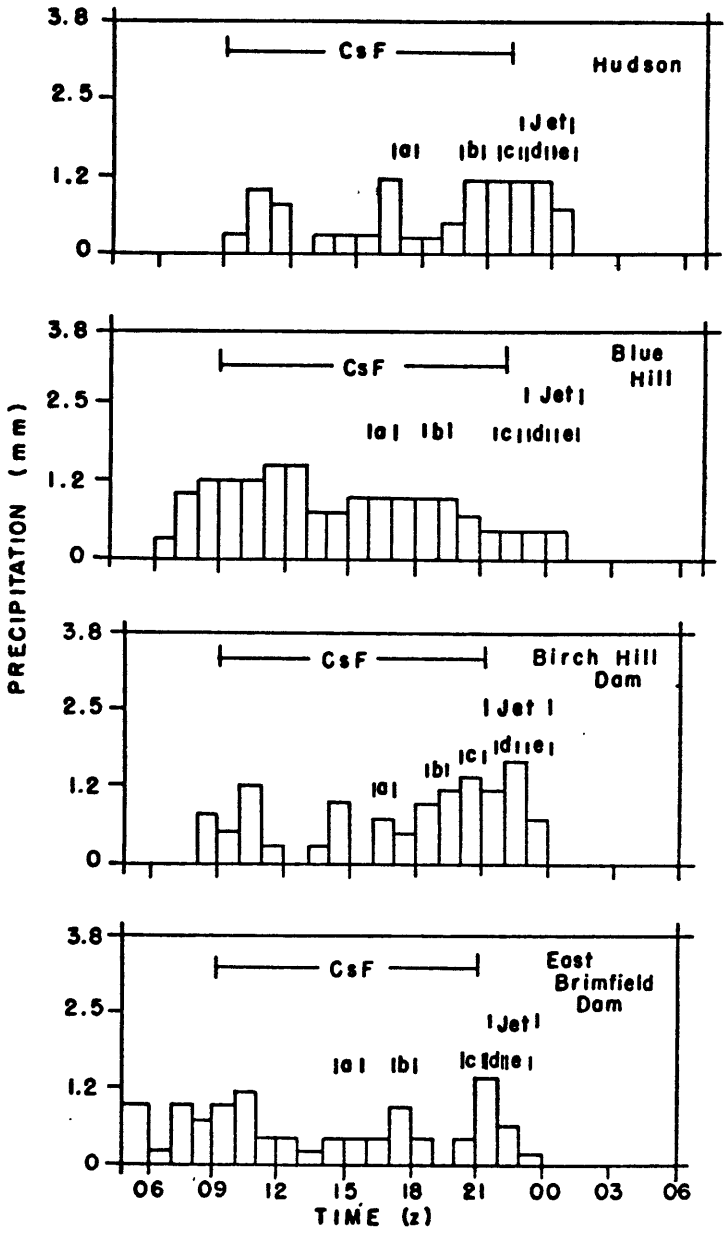

FIGURE 9: The same as Figure 6, except for the case of 15 February 1970. The times of the CsF and the jet are indicated by brackets. The two SMSA's associated with the jet are labeled (d) and (e).

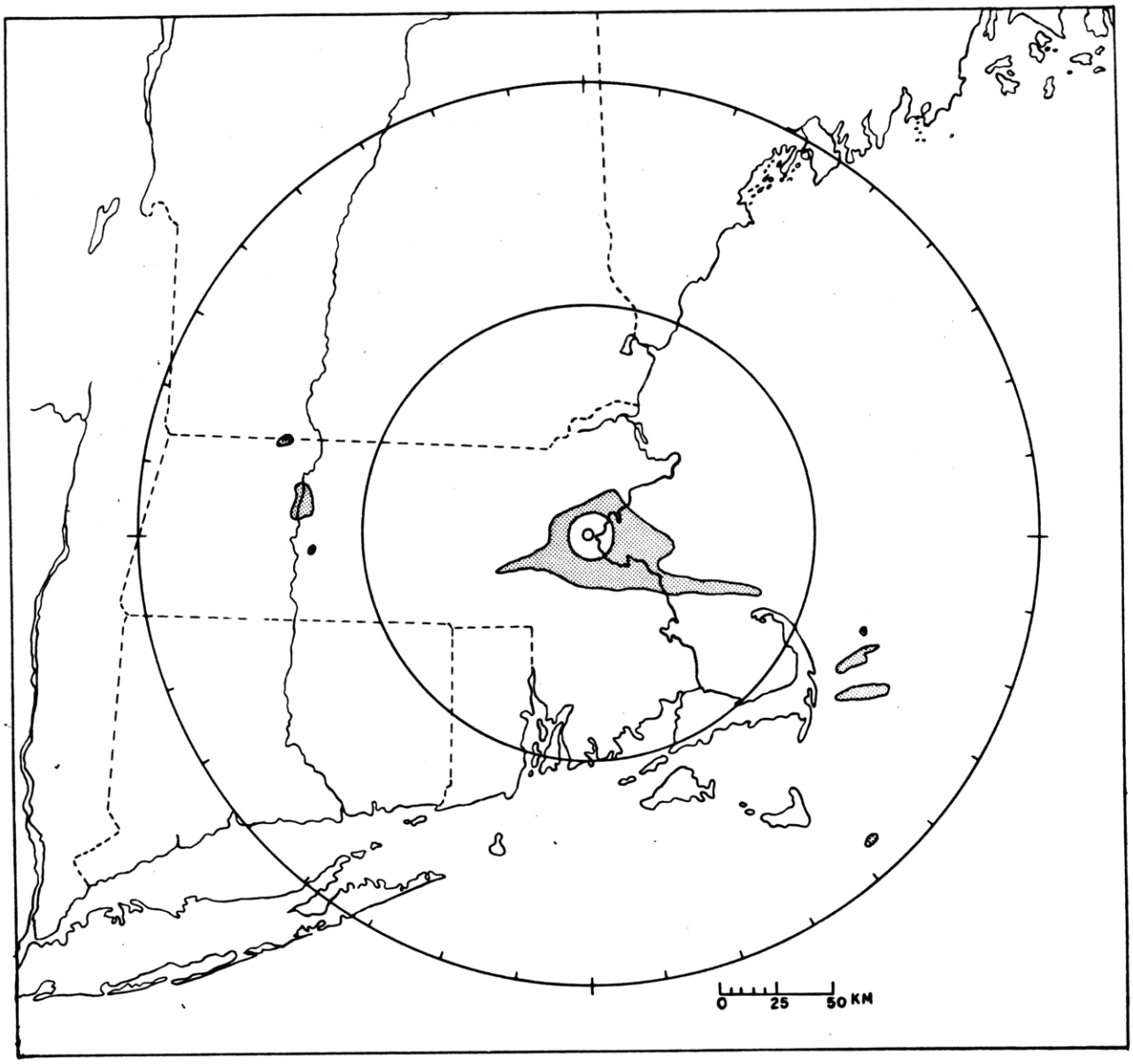

FIGURE 10: PPI tracing of SMSA over Boston at 0030Z, 24 December 1970. The circles are the same as in Figure 8. Stippling represents the threshold of the lowest intensity level.

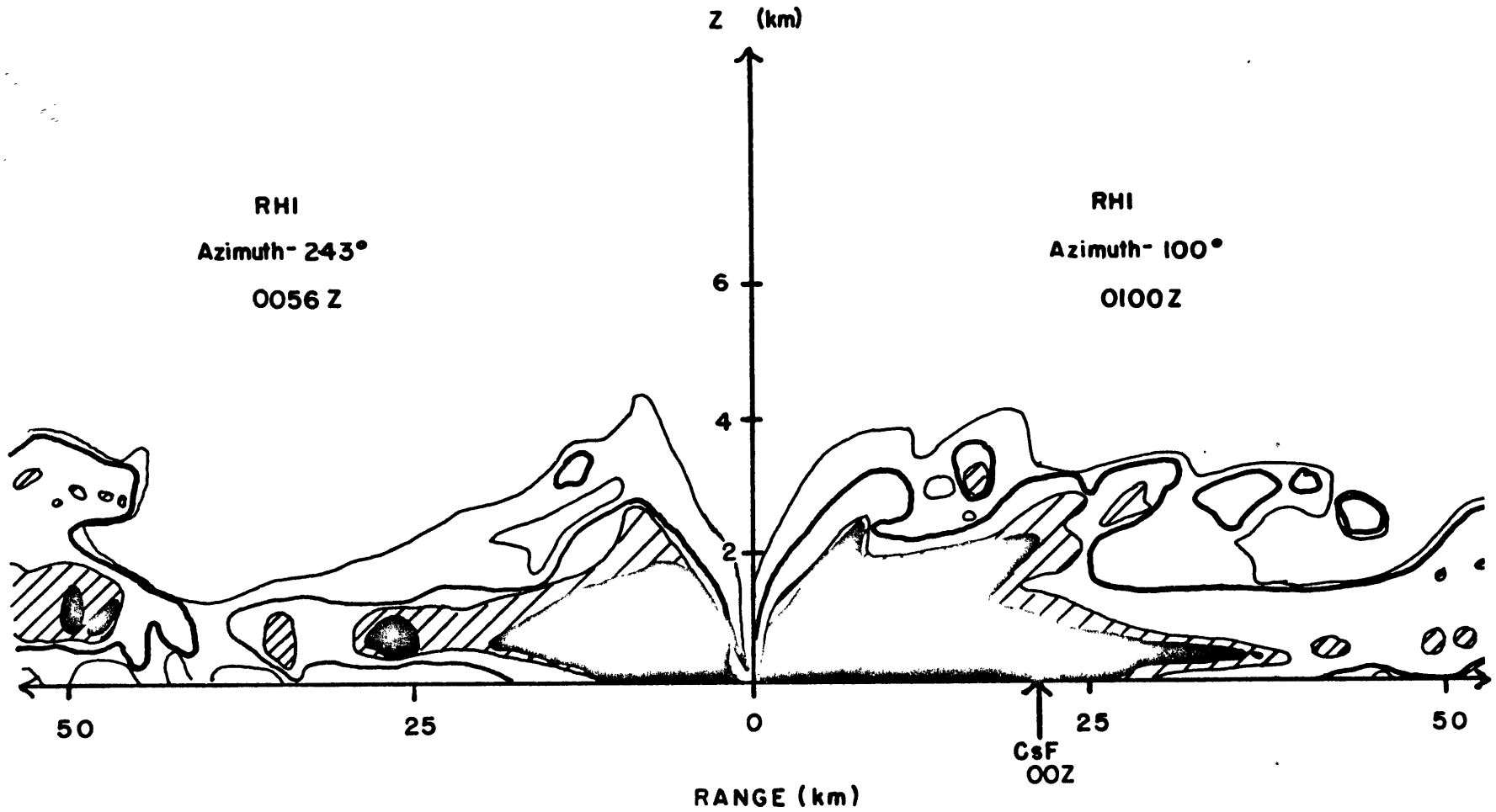

FIGURE 11: RHI-derived cross-section through SMSA for 0100Z, 24 December 1970. The abscissa is distance from the radar (km) and the ordinate is height (km). The light solid line is the threshold of intensity level one; the heavy solid line intensity level two (0.2mm hr^{-1} in snow); cross-hatching level 3 (~0.5mm hr^{-1} in snow); and solid level 4 (~5mm hr^{-1} in snow).

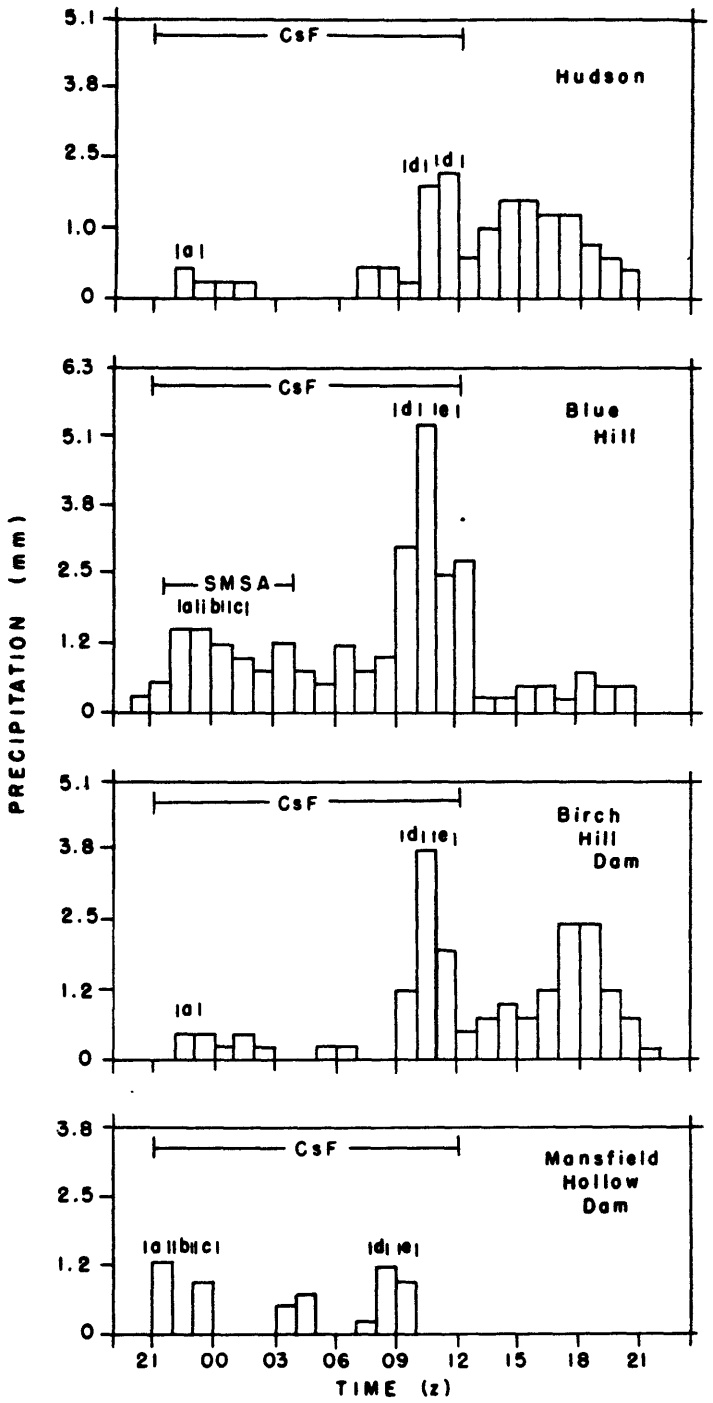

FIGURE 12: The same as Figure 6 except for case of 24 December 1970. The times of the CsF and the SMSA are indicated by brackets. Letters indicate bands that were observed.

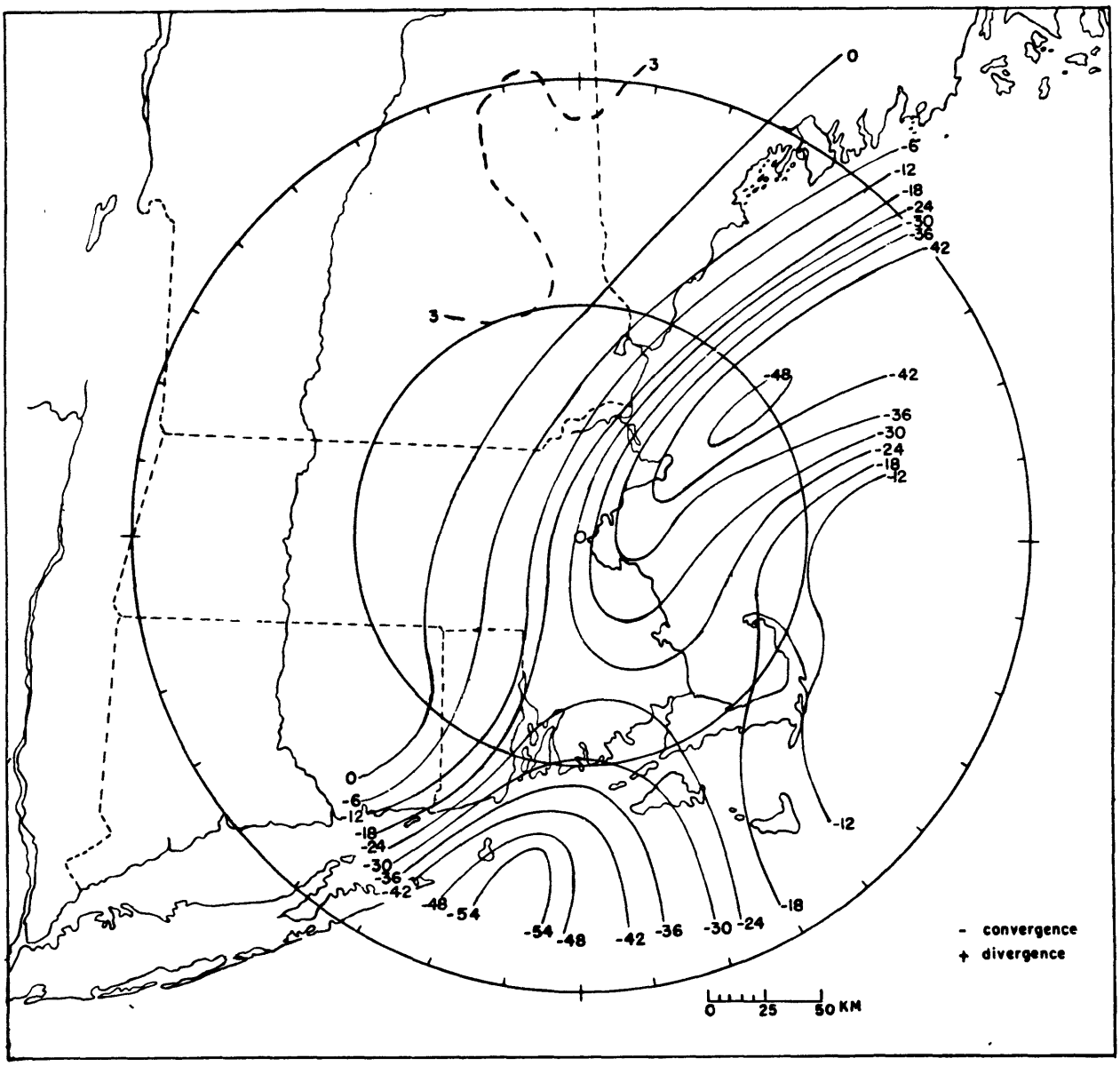

FIGURE 13: Mean water vapor divergence field over 15 hours when CsF was present for case of 24 December 1970. Solid lines represent isopleths of water vapor divergence at intervals of 6×10^{-5} g m^{-3} sec^{-1}. Positive values indicate divergence and negative values convergence.

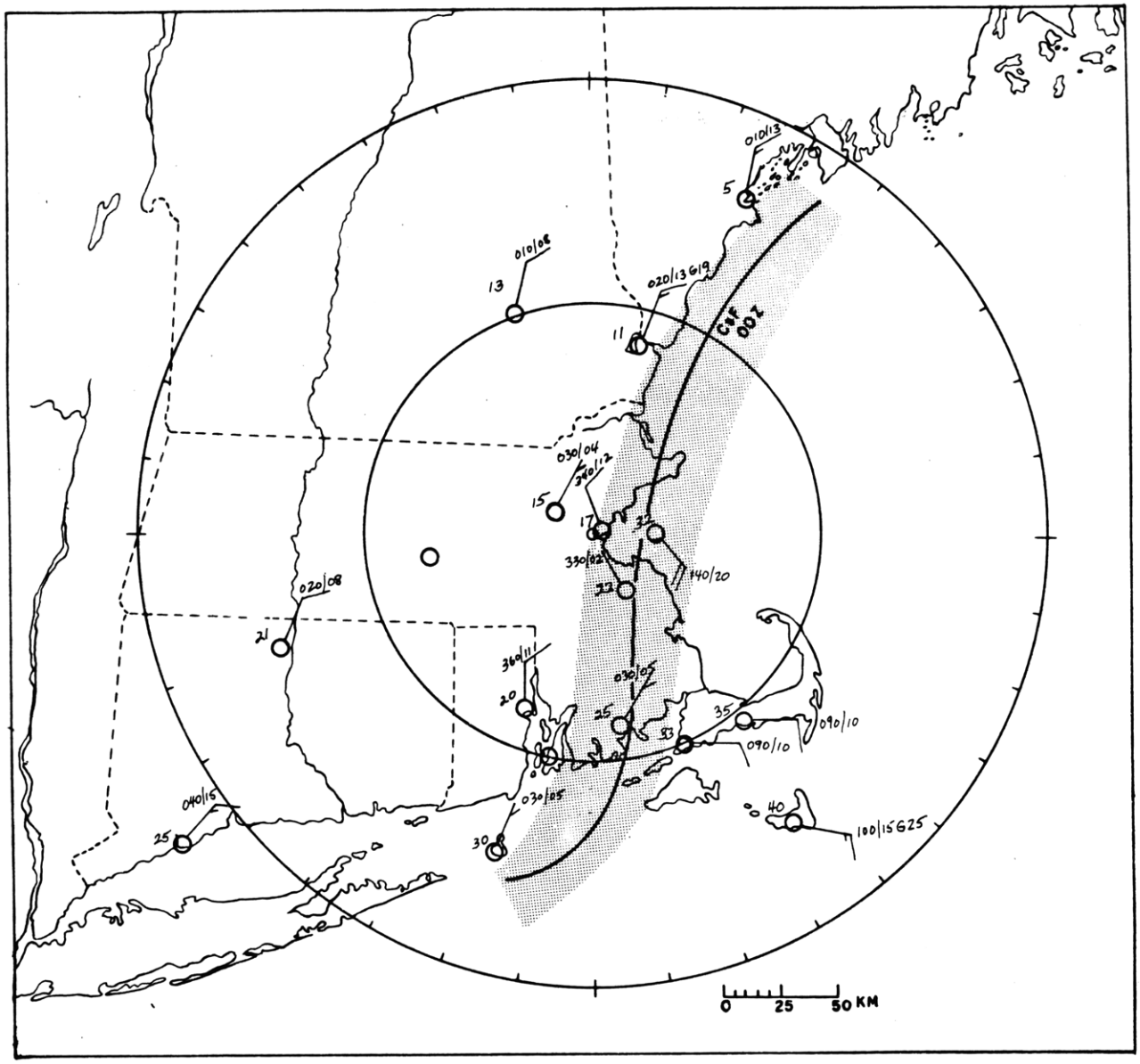

FIGURE 14: Same as Figure 4, except for 00Z, 24 December 1970.

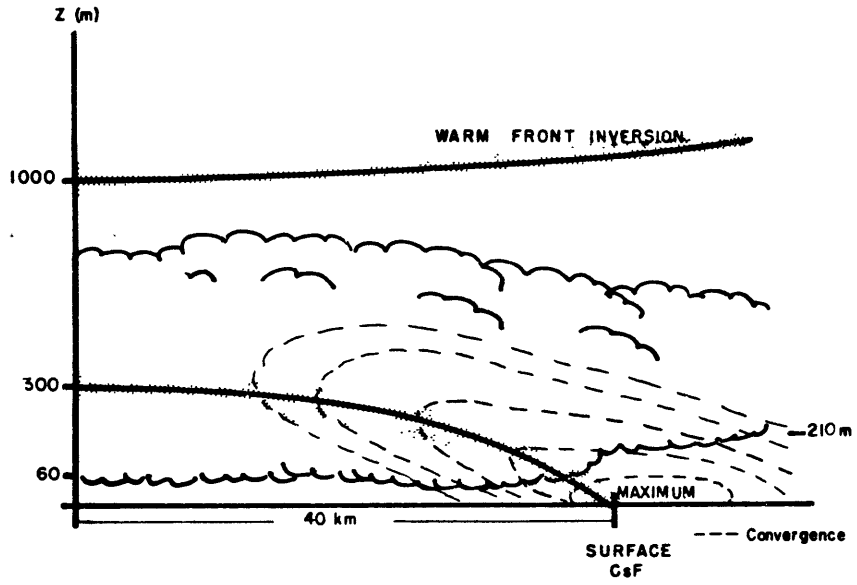

FIGURE 15: Schematic representation of cross-section through surface layer during times the CsF is present. The abscissa is distance (km) and the ordinate is height (km). The stippled areas represent the frontal zones and the broken lines represent the water vapor convergence field.

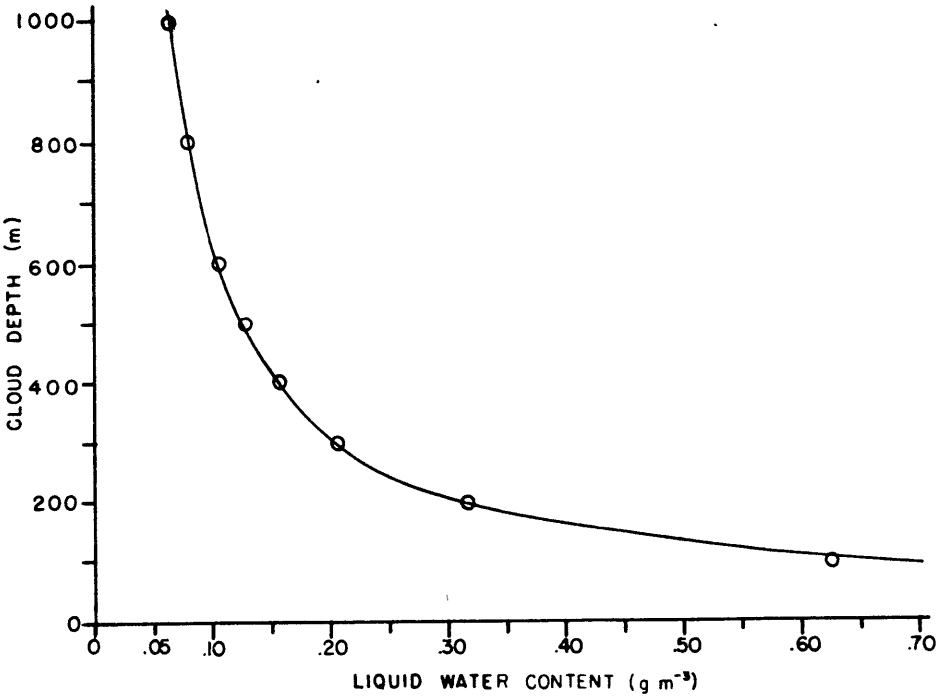

FIGURE 16: Combinations of cloud depth and mean liquid water contents, which would add 0.90mm hr^{-1} of water to an initial snowfall of 0.46mm hr^{-1}.

APPENDIX I

Characteristics of the WR-66 Radar

G - Antenna Gain	41.3 db
θ - Beam Width between half power points	1.35^{o} or 2.36×10^{-2} radians
τ - Pulse Length	1.0×10^{-6} sec.
λ - Wavelength	10.5 cm.

P_t - Peak Power transmitted - 600 Kw

(Klystron charged February 1971 - power as low as 280 Kw).

APPENDIX II

New England Coastal Front Cases (1964-1972)

Tabulated by Synoptic Type (from Bosart, 1974)

DATE	SYNOPTIC TYPE	DATE	SYNOPTIC TYPE	DATE	SYNOPTIC TYPE
1/1/64	A	12/11/67	B	12/16/70	A
3/26/64	B	12/28/67	A	12/22/70	E
3/29/64	B	12/31/67	B	12/23/70	B
9/23/64	A	1/14/68	A	1/14/71	B
10/17/64	A	11/7/68	E	10/25/71	A
1/24/65	B	11/18/68	E	11/25/71	A
2/12/65	B	12/4/68	A	12/15/71	C
2/25/65	A	12/28/68	B	12/30/71	B
12/12/65	B	1/1/69	B	2/3/72	B
1/3/66	B	2/9/69	A	2/26/72	E
1/6/66	B	12/8/69	B	3/15/72	B
3/4/66	B	12/22/69	A	11/5/72	D
10/19/66	A	12/26/69	A	11/30/72	A
12/13/66	A	2/15/70	B	12/4/72	E
1/4/67	B	11/15/70	D	12/6/72	C
1/27/67	B	12/9/70	B	12/8/72	E
4/18/67	B	12/12/70	E	12/21/72	D
11/22/67	A	12/13/70	E	12/31/72	C

APPENDIX III

Calculation of the Vertical Profiles of Equivalent Potential Temperature

The Rossby Psuedo-Equivalent Potential Temperature is computed with respect to both ice and water for all the significant levels up to 250 mb, of a standard rawindsonde ascent.

The psuedo-equivalent potential temperature (θ_e) is conserved for an air parcel undergoing dry adiabatic or psuedo-adiabatic ascent, providing several assumptions about non-adiabatic effects are justified. The time scale of the features studied was small enough to justify neglect of the variation in θ_e due to radiational cooling and heating. Neglect of the effects of mixing, within parcels, of air with different θ_e values cannot be easily justified but this mixing will be neglected.

All the water vapor that was condensed was assumed to be removed from the parcel, probably as precipitation, and the released latent heat of vaporization is used to heat the air in the parcel. When computing the equivalent potential temperature with respect to ice (θ_{ei}), it was assumed that all the water vapor that condensed was either sublimated onto ice crystals or eventually activated by the ice nuclei. This process also released the latent heat of fusion as well as the latent heat of vaporization, which also went to heat the air within the parcel. This assumption

seemed justified considering that the predominate precipitation type in all the cases was snow.

The equations used in the computations were taken from Phillips' lecture notes for dynamic meteorology (chapters 2 and 3). They are listed briefly below.

$$\theta_e = \theta \exp\left[\frac{Lv\ rs}{Cp\ T}\right] \qquad 1)$$

$$\theta_{ei} = \theta \exp\left[\frac{Ls\ rs}{Cp\ T}\right], \qquad 2)$$

where Lv is the latent heat of vaporization (which is dependent on temperature) which at 0^oC is equal to $2.501 \times 10^6\ m^2\ sec^{-2}$,

$$Ls = Lv + Lf,$$

where Lf is the latent heat of fusion (assumed not dependent on temperature) and Ls is the latent heat of sublimation equal to $2.835 \times 10^6\ m^2\ sec^{-2}$ at 0^oC, Cp is the specific heat of dry air at constant pressure equal to $1.004 \times 10^3\ m^2\ sec^{-2}\ {}^oK^{-1}$, θ is the potential temperature (^oK), rs is the saturation mixing ratio, and T is the temperature of the parcel at saturation (^oK).

APPENDIX IV

Calculation of the Mean Surface Two-Dimensional Water Vapor Divergence

For the case of 24 December 1970, the mean surface two-dimensional water vapor divergence or flux ($\nabla \cdot r\underline{V}$) was computed by combining the mean surface divergence ($\nabla \cdot \underline{V}$) calculations from Bosart (1975) with the mean observed surface water vapor content (r).

Bosart (1975) used the observed surface wind field, subjectively analyzed every three hours, to compute the divergence field. These three-hourly values were averaged over the 15 hours the CsF was present to obtain the mean divergence field for the whole period.

The water vapor field was computed from the observed dew-point temperatures subjectively analyzed for the same three-hour periods as those used by Bosart in the divergence calculations. The three-hourly values of the water vapor content were averaged, in the same manner as the divergence values, to obtain the mean water vapor field for the whole period.

These two fields were then multiplied together to obtain the mean water vapor divergence field in units of grams of water vapor per meter cubed of dry air per second. This mean divergence field is depicted in Figure 13.

APPENDIX V

Calculations of the Growth of Aggregated Snowflakes by Collection

The growth rates of aggregated snowflakes falling through a cloud of variable depth and mean liquid content are computed. The snowflakes are assumed to grow by accretion of the liquid water in the cloud. To simplify the computations the collection efficiency is assumed to be 100%. To further simplify the computations, the size distribution and fall velocities of the aggregates will be assumed to be constant throughout the collection process.

Using these assumptions, a simple equation to calculate the added water picked up by the aggregates as they pass through the cloud results. It is as follows

$$R_{add} = H\, l\, \left(\frac{\pi}{4} \times 10^{-6}\right)\, \left(\Sigma Ds^2\, N_h\right) \qquad 1)$$

where R add is the added water in g m^{-2} sec^{-1}, Ds is the diameter of the horizontal cross-section of the snowflake (mm), H is the depth of the cloud (m), l is the mean liquid water content in the cloud (g m^{-3})and N_h is the number of aggregates falling onto the surface layer of a certain diameter size, (m^{-2} sec^{-1}).

N_h is computed using a size distribution and fall velocities for aggregates given by Gunn and Marshall (1958).

The size distribution is computed using the relationship

$$N_D = No\ e^{-\Lambda D},$$

where D is the equivalent diameter of a snowflake related to Ds by the proportion constant k. The appropriate value of k was taken from Magono (1953) (for wet snow k is equal to 4.5). N_D is the number of aggregates per diameter size, and No and Λ are variables dependent on the rainfall rate, R (mm hr^{-1}). No and Λ are defined as

$$No = 3.8 \times 10^3\ R^{-0.87}$$

$$\Lambda = 25.5\ R^{-0.48}$$

N_D and No have units of m^{-3}. The R used was 0.46 mm hr^{-1}; that of the unenhanced regions for the case of 24 December 1970.

The fall velocities are given by the relationship

$$V_T = 200\ D^{0.31}.$$

For each equivalent diameter size, N_h is the product of N_D and V_T.

For these computations four equivalent diameter sizes were used. In Table A1 are the values of the various parameters for this computation.

An equation relating H and I was derived by specifying the value of R add. R add was set equal to 0.9 mm hr^{-1}, which is

the value of enhancement of the observed precipitation rate for the case of 24 December 1970.

The resulting relation is

$$I = \frac{62.5}{H} \qquad 2)$$

This relationship is depicted in Figure 16.

TABLE A1

D (mm)	N_D ($m^{-3}.5mm^{-1}$)	V_T ($m\ sec^{-1}$)	N_h ($m^{-2}sec^{-1}$)	D_s (mm)
0.5	684.0	0.8	468.0	2.2
1.0	92.5	1.0	92.5	4.5
1.5	14.5	1.1	16.0	6.8
2.0	2.3	1.2	2.8	9.0

ACKNOWLEDGEMENTS

The author would like to express sincere gratitude to Dr. Pauline M. Austin for her guidance and many valuable suggestions during the formulation of this thesis.

Special thanks go to my wife Anita, her sacrifice and encouragement have made the completion of this work possible. Also, special thanks go to Karen Kutscher and Beth Prolman for typing the final manuscript and to Mr. Steven Ricci, for his help in drafting many of the figures.

Finally, the author would like to express his appreciation to the National Science Foundation for partial support of this work under Grant No. GA 36364X.

REFERENCES

Austin, P.M. and R.A. Houze, 1972: Analysis of the structure of precipitation patterns in New England. J. App. Met., 11, 926-935.

Bosart, L.F., 1975: New England coastal frontogenesis. To be published in Quart. J. Roy. Met. Soc.

Bosart, L.F., C.J. Vaudo, and J.H. Helsdon, 1972: Coastal frontogenesis. J. App. Met., 11, 1236-1258.

Browning, K.A., M.E. Hardman, T.W. Harrold, and C.W. Pardoe, 1973: The structure of rainbands within a mid-latitude depression. Quart. J. Roy. Met. Soc., 99, 215-231.

Einandi, F. and D.P. Lalas, 1975: Wave-induced instabilities in an atmosphere near saturation. J. Atmos. Sci., 32, 536-547.

Elliot, R.D. and E.L. Hovind, 1964: On convective bands within Pacific Coast storms and their relation to storm structure. J. App. Met., 3, 143-154.

Gunn, K.L.S. and J.S. Marshall, 1958: The distribution with size of aggregate snowflakes. J. of Met., 15, 452-461.

Harrold, T.W., 1973: Mechanisms influencing the distribution of precipitation within baroclinic disturbances. Quart. J. Roy. Met. Soc., 99, 232-257.

Magono, 1953: Scientific report, Yokohama National University. Section 1, 2, 18.

Marshall, J.S. and W. Mck. Palmer, 1949: Rain and snow distribution. Paper read at the annual meeting of the R. Soc. of Canada.

Matsumoto, S. and K. Ninomiya, 1969: On the role of convective momentum exchange in the mesoscale gravity wave. J. of Met. Soc. of Japan, 47, 75-85.

Phillips, N.A.: Intro. to Dyn. Met., Lecture Notes, Dept. of Met., M.I.T.

Reed, R.W., 1972: Characteristics and development of mesoscale precipitation areas in extra-tropical cyclones. S.M. Thesis, Dept. of Met., M.I.T.

Sanders, F., 1973: Skill in forecasting daily temperature and precipitation: some experimental results. Bull. Amer. Met. Soc., 54, 1171-1179.